AL/EQ-TR-1994-0052
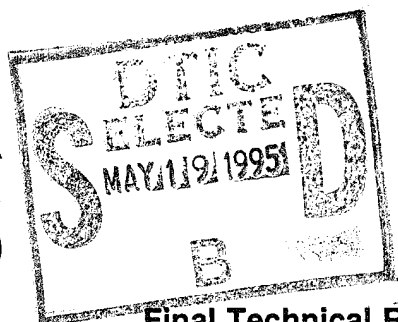
# SPRAY COATING OF METALS PHASE II
# PROOF OF CONCEPT

Scott A. Ploger, Ray A. Berry, Patricia B. Hembree,
James F. Key, Lloyd D. Watson

Idaho National Engineering Laboratory
EG&G Idaho, Inc.
Idaho Falls, Idaho 83415

ENVIRONICS DIRECTORATE
139 Barnes Drive, Suite 2
Tyndall AFB FL 32403-5323

December 1994

Final Technical Report for Period March 1989 - September 1992

**A R M S T R O N G**

**L A B O R A T O R Y**

DTIC
SELECTED
MAY 19 1995
B

19950518 027

AIR FORCE MATERIEL COMMAND
TYNDALL AIR FORCE BASE, FLORIDA 32403-5323

NOTICES

This report was prepared as an account of work sponsored by an agency of the United States Government. Neither the United States Government nor any agency thereof, nor any employees, nor any of their contractors, subcontractors, or their employees, make any warranty, expressed or implied, or assume any legal liability or responsibility for the accuracy, completeness, or usefulness of any privately owned rights. Reference herein to any specific commercial products, process, or service by trade name, trademark, manufacturer, or otherwise, does not necessarily constitute or imply its endorsement, recommendation, or favoring by the United States Government or any agency, contractor, or subcontractor thereof. The views and opinions of the authors expressed herein do not necessarily state or reflect those of the United States Government or any agency, contractor, or subcontractor thereof.

When Government drawings, specifications, or other data are used for any purpose other than in connection with a definitely Government-related procurement, the United States Government incurs no responsibility or any obligation whatsoever. The fact that the Government may have formulated or in any way supplied the said drawings, specifications, or other data, is not to be regarded by implication, or otherwise in any manner construed, as licensing the holder or any other person or corporation; or as conveying any rights or permission to manufacture, use, or sell any patented invention that may in any way be related thereto.

This technical report has been reviewed by the Public Affairs Office (PA) and is releasable to the National Technical Information Service, where it will be available to the general public, including foreign nationals.
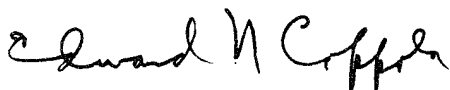
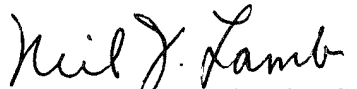This report has been reviewed and is approved for publication.

WILLIAM J. GOODEN, Capt, USAF
Project Manager

MICHAEL G. KATONA, PhD
Chief Scientist, Environics Directorate

EDWARD N. COPPOLA, Maj, USAF
Chief, Site Remediation Division

NEIL J. LAMB, Colonel, USAF, BSC
Director, Environics Directorate

# REPORT DOCUMENTATION PAGE

Public reporting burden for this collection of information is estimated to average 1 hour per response, including the time for reviewing instructions, searching existing data sources, gathering and maintaining the data needed, and completing and reviewing the collection of information. Send comments regarding this burden estimate or any other aspect of this collection of information, including suggestions for reducing this burden, to Washington Headquarters Services, Directorate for Information Operations and Reports, 1215 Jefferson Davis Highway, Suite 1204, Arlington, VA 22202-4302, and to the Office of Management and Budget, Paperwork Reduction Project (0704-0188), Washington, DC 20503

| 1. AGENCY USE ONLY (Leave blank) | 2. REPORT DATE<br>December 1994 | 3. REPORT TYPE AND DATES COVERED<br>Final Report Thru Sep 92 |
|---|---|---|

**4. TITLE AND SUBTITLE**
Spray Coating of Metals Phase II: Proof of Concept
Final Report

**5. FUNDING NUMBERS**
DOE Contract No.
DE-AC07-76ID01570

**6. AUTHOR(S)**
Scott A Ploger, Ray A Berry, Patricia B. Hembree,
James F. Key, Lloyd D. Watson

**7. PERFORMING ORGANIZATION NAME(S) AND ADDRESS(ES)**
Idaho National Engineering Laboratory
EG&G Idaho, Inc
Idaho Falls, Idaho 83415

**8. PERFORMING ORGANIZATION REPORT NUMBER**
AL/EQ-TR-1994-52

**9. SPONSORING / MONITORING AGENCY NAME(S) AND ADDRESS(ES)**
AL/EQS-OL
139 Barnes Drive, Suite 2
Tyndall AFB FL 32403-5323

**10. SPONSORING / MONITORING AGENCY REPORT NUMBER**

**11. SUPPLEMENTARY NOTES**
Technical Representative: Capt William J. Gooden
DSN: 523-6239
Comm: (904) 283-6239

**12a. DISTRIBUTION AVAILABILITY STATEMENT**
Approved for public release. Distribution unlimited.

**12b. DISTRIBUTION CODE**

**13. ABSTRACT (Maximum 200 words)**

A spray coating technique is being developed to replace electroplating processes at Air Logistics Centers and thereby reduce hazardous wastes. A bench-scale spray system was used to coat low-carbon steel strips with three cobalt-chromium hardfacing alloys. The process shows promise to be a replacement for chromium electroplating. One-dimensional models incorporating the most fundamental aspects of molten metal nebulization and coating deposition provided physical insight on the process.

**14. SUBJECT TERMS**
Spray Coating, Electroplating, Metal Finishing

**15. NUMBER OF PAGES**

**16. PRICE CODE**

| 17. SECURITY CLASSIFICATION OF REPORT<br>UNCLASSIFIED | 18. SECURITY CLASSIFICATION OF THIS PAGE<br>UNCLASSIFIED | 19. SECURITY CLASSIFICATION OF ABSTRACT<br>UNCLASSIFIED | 20. LIMITATION OF ABSTRACT<br>UL |
|---|---|---|---|

# PREFACE

This report was prepared by Idaho National Engineering Laboratory, EG&G Idaho, Inc., Idaho Falls, Idaho 83415 for the Armstrong Laboratory Environics Directorate (AL/EQ), Suite 2, 139 Barnes Drive, Tyndall AFB, Florida 32403-5319.

This final report describes a laboratory system for spray coating of metals, laboratory testing of three cobalt-chromium hardfacing alloys, analysis of the potential for the spray coating system to replace chromium electroplating at Air Logistics Centers and recommendations for continued development of the process.

| Accession For | |
|---|---|
| NTIS GRA&I | ☑ |
| DTIC TAB | ☐ |
| Unannounced | ☐ |
| Justification | |
| By | |
| Distribution/ | |
| Availability Codes | |
| Dist | Avail and/or Special |
| A-1 | |

iii

(The Reverse of This Page is Blank)

# EXECUTIVE SUMMARY

## A. OBJECTIVE

The purpose of this document is to present results from a Phase II proof of concept study for spray coating metal parts as a replacement for chromium electroplating.

## B. BACKGROUND

Strong environmental and occupational health regulatory driving forces are increasingly restricting chromium electroplating. The Controlled Aspiration Process is a spray coating process that is a candidate for replacing chromium electroplating. In the process, molten metal is drawn by suction into a converging/diverging nozzle. The metal is sheared into fine droplets by the inert carrier gas. Droplets of molten metal are carried to the base metal where they consolidate and solidify into a dense coating. The part is sprayed in a chamber which allows for an inert atmosphere and isolates personnel from safety hazards. The process does not produce any aqueous wastes and overspray particles are easily filtered.

## C. SCOPE

This report documents the design, fabrication and testing of a bench scale Controlled Aspiration Process system. It also documents computer simulations of nozzle dynamics and droplet consolidation. Three cobalt chromium alloys were tested. Porosities varied between 0 and 5% and were not interconnected. Higher spray alloy carbon content, which forms carbides in the coating, influences microhardness and brittleness. Brittle fractures were present in several samples. Coatings on some samples ruptured, fractured or delaminated during adhesion testing. The temperature required for spraying pure chromium exceeded the materials limitations of the bench system. Resistive heating elements proved incapable of achieving temperatures needed to ensure deposition of droplets in the liquid state and were replaced by inductive heating elements. The nozzle configuration was a rectangular design with multiple orifices. Differences in metal temperature and flow rates between the orifices plagued nozzle operation. Experimental results suggest that finding and maintaining optimum temperatures and a more effective nozzle design, combined with possible changes in the spray alloys, can overcome these difficulties.

## D. CONCLUSIONS

Spray coating has potential as a non-polluting replacement for chromium electroplating at Air Logistics Centers, but will be limited to line-of-sight applications. This effort significantly advanced the state of the art and highlights the promise of the Controlled Aspiration Process to replace chromium electroplating. However, the capability to produce consistent uniform coatings has yet to be demonstrated.

## E. RECOMMENDATIONS

Future work should emphasize improving coating properties, in particular adhesion and elimination of fatigue cracking, and obtaining consistent uniform coatings. Nozzle configuration should be changed to a circular design with a single orifice. Key parameters for study are base metal preparation and temperature, alloy composition, nozzle design, carrier gas flowrate/pressure, carrier gas temperature, chamber gas temperature, liquid metal temperature, droplet size and droplet velocity. Nozzles fabricated from materials that are more durable than boron nitride should be tested after completion of nozzle design studies. Recirculation of argon gas and use of nitrogen need to be evaluated for most economical process operation.

(The Reverse of This Page is Blank)

# TABLE OF CONTENTS

# TABLE OF CONTENTS
## (CONCLUDED)

## LIST OF FIGURES

# LIST OF TABLES

x

# SECTION I
## INTRODUCTION

Electroplating and metal finishing produce hazardous wastes, with cleanup and disposal costs of millions of dollars each year. A practical solution to this problem is to develop alternative metallization processes that reduce or eliminate hazardous waste.

## A. OBJECTIVE

The objective of the Spray Coating of Metals project is to minimize the generation of hazardous wastes by developing an alternative to electroplating. During Phase I, ductile tin coatings were successfully sprayed onto low-carbon steel. The molten metal-to-deposit conversion efficiency was high. Strong mechanical bonds produced good adhesion to the grit-blasted base metal, while coating layer strength was improved by rapid solidification. Phase II of this project, jointly funded by the United States Air Force and the Department of Energy, involved upgrading the bench-scale apparatus to spray high melting point metals and investigating the replacement of chromium electroplates with sprayed chromium or chromium-bearing alloys.

## B. BACKGROUND

Electroplating, which is frequently used to produce corrosion resistant coatings, is an expensive, waste-producing operation. Many of the elements in the electroplating baths (e.g., Cr, Ni, Cd, Pb) are hazardous materials, and personnel safety precautions as well as wastewater treatment or disposal are costly. In addition, electroplating is generally restricted to pure elemental coatings by the dissimilar plating behaviors of different ionic species.

Spray forming of metallic coatings with the Controlled Aspiration Process being developed at the Idaho National Engineering Laboratory (INEL)

1

generates much less, if any, hazardous waste. In this nebulization process, molten metal is drawn by aspiration into the throat of a converging/diverging gas nozzle, much as in a venturi carburetor. The liquid stream is sheared by the gas flow into a spray of individual droplets that quickly cool, in flight, from both convection and radiation. Before complete solidification occurs, however, the droplets collect on the surface to be coated. Coatings can be sprayed directly from the melt with over 99 percent conversion efficiency, and any overspray can be collected and recycled.

In contrast to conventional electroplating processes, the composition of a spray formed coating is dictated solely by the melt composition. Thus, for example, pure chromium electroplates can probably be replaced by alloy coatings with relatively low chromium content but superior resistance to wear, galling, and corrosion. This flexibility in materials selection may eliminate some hazardous substances from the coating process. It may also reduce U.S. dependence on foreign sources for some strategic elements.

Preliminary research indicates that, after scaleup, INEL nebulizers will spray wide, uniformly thick coatings with negligible porosity. The dimensional control thus afforded may minimize subsequent grinding to tolerances, and thus reduce hazardous airborne contaminants and related personnel exposure farther down the production line. Spray forming also offers the benefits of rapid solidification. Spray formed metals can usually be made stronger and harder than conventionally processed materials due to their small grain sizes, the freezing of metastable alloy phases, and negligible defect formation from impurity segregation. Furthermore, spray forming technology allows conventional coatings to be replaced with microcrystalline or metallic glass layers, which have unparalleled corrosion and erosion resistance. Advanced coatings could significantly reduce the frequency at which U.S. Air Force components must be stripped and recoated.

2

## C. SCOPE/APPROACH

Phase II consisted of the design, construction, and testing of a laboratory-scale spray coating system to replace chromium electroplating. This involved (a) upgrading the Phase I system to handle the elevated temperatures necessary to spray metals with properties equal to or surpassing those of electroplated chromium; (b) determining the adhesion strength, hardness, porosity, and thickness uniformity of coated specimens to assess overall coating quality; (c) studying base metal surface preparation to confirm that grit-blasting or shot-peening can eliminate the pickling and cathodic cleaning steps currently required for chrome plating (as well as hydrogen pickup and the post-plating annealing step); and (d) numerically modeling two-phase nozzle and plume dynamics to better understand nebulizer design features and operating characteristics. Experimental measurements were made in English units; modeling employed SI units. Phase II consisted of ten interrelated tasks, namely:

1. Task 1: Initiate Modeling Efforts for Particle Consolidation

   o Review Phase I droplet consolidation results for modeling input.

   o Outline any supporting experiments needed for modeling studies.

   o Review available models and evaluate their potential for numerically simulating the deposition of coatings.

2. Task 2: Develop High Temperature Nebulizer Assembly

   o Design and build nozzles and nozzle/tundish assemblies for high temperature operation.

   o Characterize and test nozzles and nozzle/tundish assemblies at high temperature operating conditions.

3. Task 3:  Initiate Modeling Efforts for Nozzle Dynamics

   o · Begin numerical simulations of two-phase nozzle dynamics and
      incorporate Phase I data on liquid breakup and plume geometry.

   o  Incorporate Task 2 results on nozzle characterizations with
      high temperature gas flows and mass loading of gas streams.

4. Task 4:  Test High Temperature Spray System

   o  Perform operational checks on instrumentation for diagnostic
      measurements and controlling component parameters over desired
      ranges of temperatures.

   o  Verify hardware/computer interfaces, computer software
      packages, and calibration modes of instrumentation.

5. Task 5:  Perform Initial Coating Trials

   o  Spray coat a high melting point material onto a steel specimen;
      if necessary, revise spray system features to improve nebulizer
      operation, plume characteristics, and deposition behavior.

   o  Coat steel specimens using a wide range of process variables.

   o  Select spray conditions likely to produce high quality
      coatings.

6. Task 6:  Analyze Preliminary Coating Specimens

   o  Visually evaluate all specimens coated in Task 5 and extract
      samples for detailed studies.

   o  Subject samples to metallography and adhesion tests to generate
      data on coating quality attributes such as porosity, thickness

uniformity, microhardness (for potential wear resistance), and bond strength.

o   Correlate results with Task 5 spraying conditions, and design an experiment to establish near-optimal spray parameters for producing desired coating properties.

7.  **Task 7:  Optimize Individual Coating Properties**

o   Spray coat steel specimens in accordance with variables specified by the experimental design selected in Task 6, while minimizing any time-dependent influences.

8.  **Task 8:  Evaluate Coated Specimens and Map Property Responses**

o   Evaluate all specimens from Task 7 in terms of potential wear resistance, microhardness, bond strength, porosity content, and coating thickness uniformity.

o   Correlate results with spraying parameters to map coating process response for each coating property measured.

o   Incorporate results into modeling efforts of Tasks 1 and 3.

o   Select a second experimental design to map property responses at finer resolution, thereby enabling accurate assessments of overall coating quality.

9.  **Task 9:  Optimize Total Coating Quality**

o   Spray coat steel specimens in accordance with variables specified by the experimental design selected in Task 8, while minimizing any time-dependent influences.

10. Task 10: Analyze Final Specimens to Fully Optimize Coating Process

o  Evaluate all specimens from Task 9 for bond strength, potential wear resistance, porosity content, and thickness uniformity.

o  Correlate results with spray system operating conditions to produce a fully optimized coating process for high temperature materials on a small scale.

o  Incorporate results into modeling effort to estimate behavior and costs of the spray coating technique for pilot-scale applications.

# SECTION II
# SPRAY SYSTEM DEVELOPMENT

## A. INTRODUCTION

As outlined above, Phase II required designing, building, and testing a system capable of spraying metals with high melting points. INEL-designed nebulizers possess fundamental operational and geometric advantages for spraying uniform metal deposits. In addition, the unique features of the controlled aspiration process allow tailoring of spray plume characteristics for demanding applications, such as coatings that will surpass U.S. Air Force standards and, at the same time, dramatically reduce hazardous wastes. Coating requirements addressed in this work include tight adherence to the base metal, full consolidation (to resist corrosion, a coating must not have any connected porosity), and uniform thickness (to minimizes subsequent grinding or machining to dimensional tolerances).

The approach adopted for development of spray forming emphasizes parametric versatility and control. Primary process variables, such as pressure, flow rate, and temperature of the nebulizing gas, are carefully monitored to control important plume characteristics, such as gas/metal mass ratio, droplet size distribution, and spatially consistent mass impingement pattern (Reference 1). Governing such features is critical for complete droplet consolidation upon impacting the base metal. Uniform wetting of the base metal by droplets at the leading plume edge is also essential to avoid interfacial porosity, which can cause coating delamination.

The nebulizing system also permits temperature control at various stages, i.e., the furnace (superheating the molten metal), nozzle/tundish assembly, gas delivery manifold, and base metal itself. This flexibility enables deposits of varying thicknesses to be sprayed over wide ranges of operating conditions. The inherent process flexibility also allows latitude in secondary aspects, including overall energy expenditure,

7

nebulizing gas recycling, and selection of component materials for lowest cost and ease of fabrication.

Nebulizer parameters can then be optimized for specific applications. For example, the extent to which a base metal can be directly heated is often constrained by the need to preserve its mechanical properties (excessive heating might anneal out hardness in high strength steels). Spray formed droplets cool in flight by radiation and convection, which restricts heat transfer to the coated surface and leaves the base metal bulk relatively cool. Yet, under proper operating conditions, the incident droplets wet the base metal surface, consolidate into a high density deposit, and produce an adherent coating through mechanical interlinkage between interfacial surfaces so that high temperature metallurgical bonding is not needed.

The patented converging/diverging nebulizer design (Reference 2) of Phase II uses a slot-type configuration with a rectangular cross section that is ideal for spraying flat metal parts. This configuration holds the most promise for restoring worn components by rapidly depositing uniform coatings over large surface areas. It also requires no flight distance for plume expansion, therefore offering the highest overall cooling rates for maximum rapid solidification benefits.

Phase II involved major increases in melt temperature of the sprayed material to handle chromium and high performance chromium alloys. Because of their substantially lower melting points, chromium alloys were sprayed first, while component heating capabilities were steadily increased in preparation for spraying elemental chromium. (Cobalt-chromium-tungsten alloys also have the potential of much greater wear resistance than electroplated chromium.) As with Phase I, this work was performed on a bench scale for an economical proof of principle.

## B. SPRAY SYSTEM CONFIGURATION

The major components of the high temperature spray coating system, except the electronics, are displayed in Figure 1. The furnace and melt delivery system performed almost exactly as designed, and no unexpected problems surfaced during its use. Crucible charges of 60 grams were adequate for all of the experiments conducted, and charges up to 150 grams could easily have been accommodated. The tilt mechanism worked smoothly and reliably throughout Phase II, with no instances of spillage when pouring into the nozzle tundish.

A regulated flow of inert argon gas is fed into the horizontally-oriented gas heater. After reaching the desired temperature, the argon enters a converging/diverging nozzle. Metal melted in the furnace is
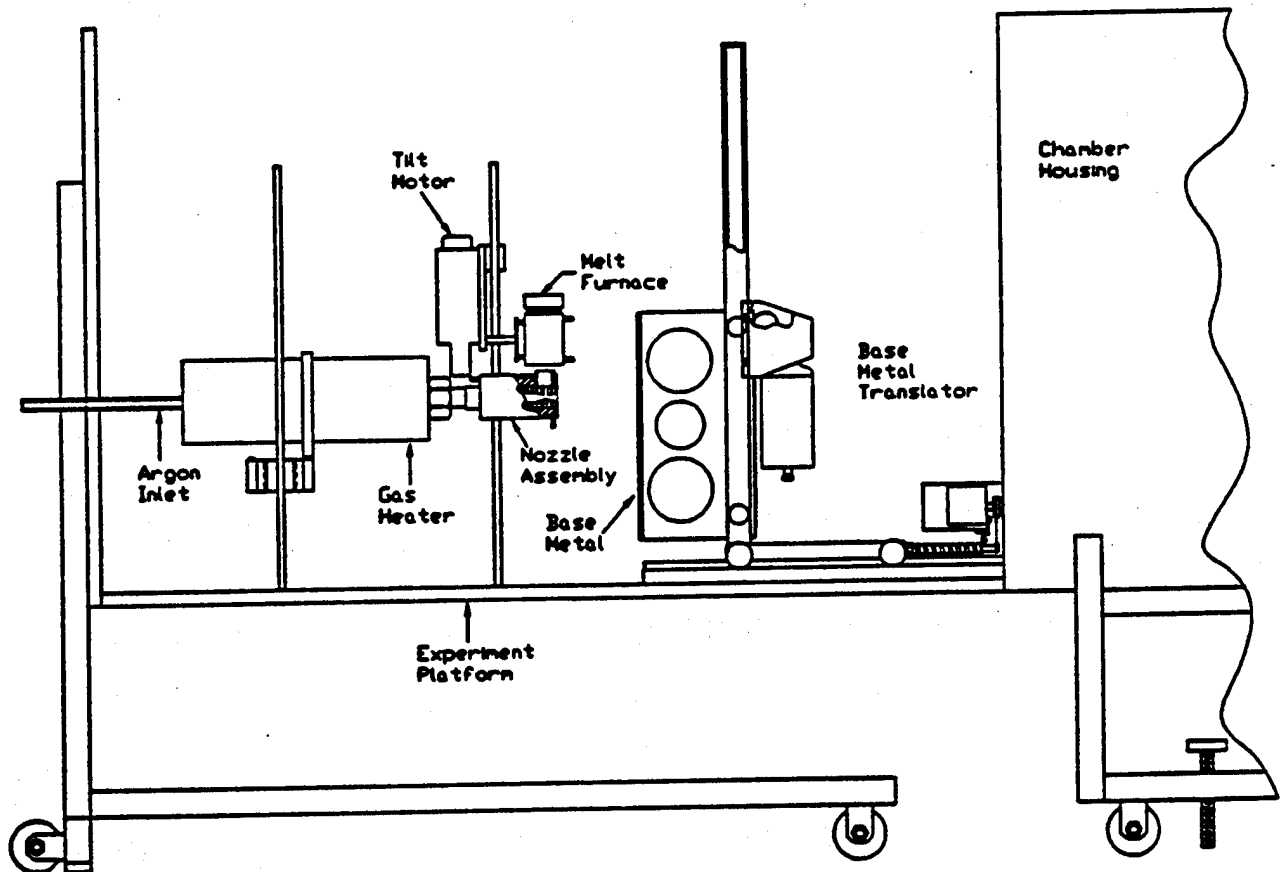


**Figure 1. Major Components of High-Temperature Spray Coating System; Chamber Housing Moved to Enclose Platform during Spraying.**

poured into a tundish immediately above the nozzle throat. With the
controlled aspiration process, the liquid metal is drawn through multiple
orifices into the nozzle throat over a narrow range of relatively low gas
pressures--typically 18 to 24 pounds per square inch absolute (psia). The
nozzle throat provides a confined interaction zone where the liquid metal
is efficiently nebulized into a directed mist of fine droplets. After a
short flight, the droplets impact the vertical metal coupon, whose position
is controlled by the translator. Under appropriate operating conditions,
the droplets consolidate into a dense, adherent coating.

All components were mounted on a movable horizontal platform that fit
inside the main chamber housing. Nebulization occurred within the closed
chamber, both for personnel safety and to reduce oxidation of hot metal,
including the gas heating elements. Inert purge gas was used to reduce
oxygen levels inside the chamber prior to heating, as well as to sweep any
unconsolidated particles (overspray) into a filter bank in the exhaust
system. Particulate concentrations were measured before and after
filtration by laser aerosol spectrometers.

## C. MEASUREMENT AND CONTROL ELECTRONICS

Considerable instrumentation was necessary to control the nebulization
process, to acquire on-line data, and to analyze dynamic influences on
coating quality. Measurement sensors included pressure transducers
upstream and downstream of the gas heater; a gas flow meter upstream of the
chamber; thermocouples in the melt furnace, nozzle body, gas heater outlet,
and on the base metal; and a drive-mechanism encoder to monitor the speed
of base metal movement. For certain experiments, temperature signals were
also fed to a gas heater controller, operated by a silicon-controlled
rectifier (SCR) circuit. In other cases, heater elements were operated
manually by individual variable transformers. Nozzle and melt furnace
temperatures were controlled manually at the induction power supply. Data
on particulate sizes and concentrations were recorded on chart outputs from
the two laser aerosol spectrometers located near the chamber exhaust.

All signals were routed through a patch panel and low-noise cables to signal conditioners for amplification and noise isolation. In addition to periodic inspection and recertification, in-place computer calibration techniques confirmed that the sensors, conditioners, and thermocouples were functioning properly. The thermocouples were tied to a cold reference junction for maximum accuracy.

Two Compaq portable computers were used for data acquisition, one for temperature data and the other for all remaining signals. Their features included a 12-megaHertz 80286 microprocessor (Intel Corp.), a 40-megabyte fixed disk drive, a 1.2-megabyte diskette drive, 640 kilobytes of random-access memory, and both serial and parallel interfaces. A versatile software package called Labtech Notebook streamlined data acquisition, as well as baseline characterization of spray system components and in-place calibrations. Data were recorded in English units.

The data acquisition system was an indispensable part of the experimental apparatus. Besides displaying and recording essential information during each experiment, the data acquisition system was invaluable for characterizing the performance of each component.

D. NEBULIZING GAS HEATER

Past INEL spray forming research found it highly desirable to heat the nebulizing gas, before it reached the nozzle. The main reason was to provide an extra degree of freedom for precise control of the nebulizing process. Heating the nebulizing gas allowed a lower nozzle temperature and less superheat in the molten metal without metal freezing in the liquid orifices. This can be especially significant for spraying high melting point metals, because nozzle and crucible degradation increases with increasing melt temperature. In addition, because gas is blown through the nozzle before spraying, the hot gas jet preheats the base metal, which may improve wetting and lower product interfacial porosity.

Phase I was conducted with a single-element, resistive gas heater wound with nichrome wire. This gas heater operated almost flawlessly for the small Phase I nozzle and the relatively low argon flow rates required. Its capacity was also adequate for preheating the cylindrical rotating base metal specimens used in most of Phase I. At the start of Phase II, incorporation of multiple nichrome elements of the same Leister design into a larger resistance-wound gas heater was attempted. However, early testing of twin nichrome elements at the power levels necessary for Phase II uncovered several problems. Therefore, it was decided to seek a commercial heater with ample power and an alternative element material. Ultimately, a 36-kilowatt heater with six iron-based elements (the "Superserp X") was purchased from GTE Sylvania, Inc. Unfortunately, several problems eventually forced numerous modifications to the standard GTE design.

Two different gas heaters of the same basic design were employed. The first used iron-based elements to raise inert gas temperatures to between 600 and 730°C at the nozzle inlet. The iron-based element design was used for most of the experiments with cobalt-chromium alloys. Later experiments with higher molten metal temperatures required tungsten elements; tungsten elements were essential for the pure chromium trial where argon temperatures were increased to approximately 1200°C. These gas heaters operated at inlet pressures of 12.4 (ambient) to 40 psia and flows from 0 to 30 standard cubic feet per minute (scfm).

The gas heater design shown in Figure 2 was developed over several months of testing and modification of the GTE heater. Six elements were oriented in a hexagonal array. Inert gas entering the heater was routed through the inlet plenum in approximately equal proportions to the six flow tubes (mullite ceramic with iron-based elements, high purity alumina with tungsten elements). Argon temperatures were monitored by thermocouples positioned near the individual tube outlets.

The first modification involved the gas inlet of the heater. Element outlet temperature measurements confirmed that gas was not equally routed to the elements (gas actually flowed backwards through the two elements

12
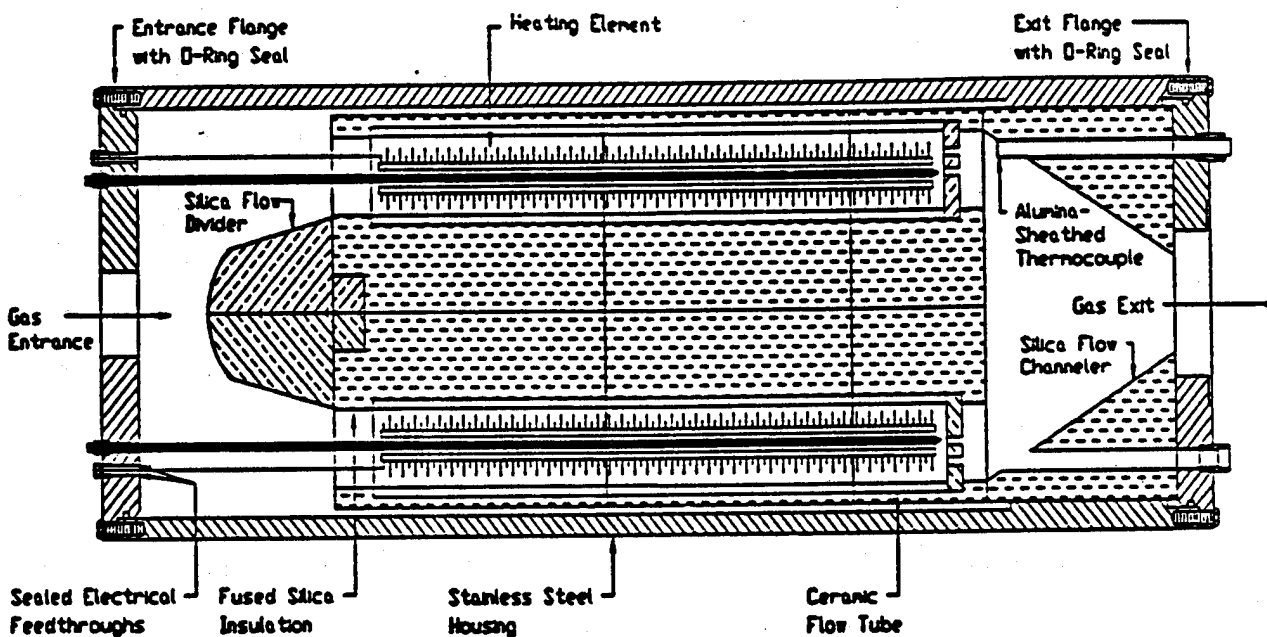
**Figure 2. Cross Section of Multiple-Element Gas Heater.**

farthest from the inlet). A concentric inlet and flow divider were built and installed to properly balance flows.

Because the heat capacity of argon is lower than that of air or nitrogen, the gases for which this heater is most frequently used commercially, the argon removed only about one-half the normal amount of heat from the elements. Furthermore, the six elements were packed tightly inside a small diameter housing with little insulation around the flow tubes. Consequently, when attempts were made to heat argon to 700°C, excessive heat was lost to the housing and hot spots formed between adjacent elements, resulting in extensive degradation of the ceramic flow tubes. Providing more separation and insulation required custom fabrication of an entirely new housing.

## E. FURNACE AND NEBULIZER

Molten metal was supplied to the nebulizer (nozzle/tundish assembly) by an induction furnace. As indicated in Figure 3, a zirconia crucible was surrounded by a graphite susceptor that was heated by the copper induction coil cast in a coarse-grained refractory cement. The service life of the

furnace crucible was heavily dependent upon melt temperature. The first
crucible survived approximately thirty experiments in the 1600 to 1700°C
range with only gradual cracking in the pour spout area. This crucible
finally failed by intergranular absorption of metal within crucible walls
and subsequent formation of cracks during cooldown. The next crucible
lasted for approximately ten trials in the 1800 to 1900°C range, whereupon
the zirconia was reduced by both the adjacent graphite susceptor and the
molten metal. Reduction created a ZrO phase that both softened the
crucible structurally and made it more prone to metal absorption.
Crucibles used near the end of Phase II in the neighborhood of 2100°C could
be trusted for only one or two trials. Late in Phase II, a boron nitride
liner was inserted between the graphite susceptor and zirconia crucible to
limit reduction of the zirconia by the graphite.

The insulating cap placed over the furnace after charging had a
centrally located hole that supported an alumina-sheathed thermocouple.
The thermocouple rested on the crucible base without contacting the walls,
thereby providing an accurate reading of metal temperature instead of
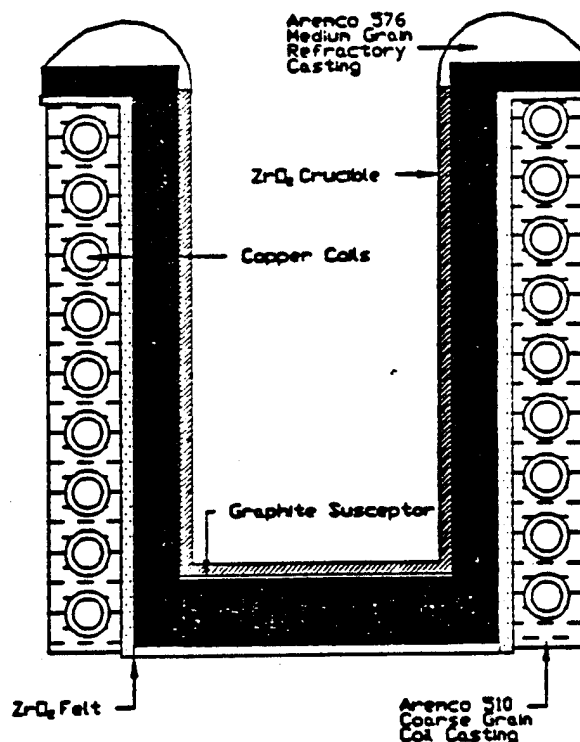


Figure 3. Cross Section of Inductively Heated Melt Furnace.

14

crucible temperature. Type C tungsten/tungsten-rhenium thermocouples were reliable up to 2000°C and most failures were traceable to degradation of the alumina sheaths by deformation, thermal fracturing, or melt dissolution.

The configuration of the nebulizer is shown in Figure 4. A metal connector was employed to join the gas heater to the ceramic nozzle body. Insulation provided by the connector's ceramic liner allowed most of the experiments to be conducted with a Type 316 stainless steel connector. However, a molybdenum connector was used toward the end of the project when high nozzle body temperatures and associated heat conduction threatened to soften the stainless steel.

The nozzle bodies were made from boron nitride, which was surrounded by conductive graphite for induction heating. The length and thickness of the susceptor were varied according to the desired heatup rate. Induction coil geometry was also changed on occasion to raise nozzle temperatures. The tundish extension (funnel) contained graphite on one side to maintain molten superheat while pouring. An annular heat shield was placed near the susceptor to limit radiant heating of the connector. A similar shield was used over the nozzle exit to reduce radiant losses there.



Figure 4. Cross Section of Inductively Heated Spray Nozzle and Gas Entrance Connector.    15

Nozzle bodies were fabricated from Combat AXO-5 (Standard Oil Engineered Materials Co.), which was selected for its consistently superior combination of mechanical and thermal properties. The main advantage of this material was its reliance on high temperature sintering and thermal curing, instead of chemical binding.

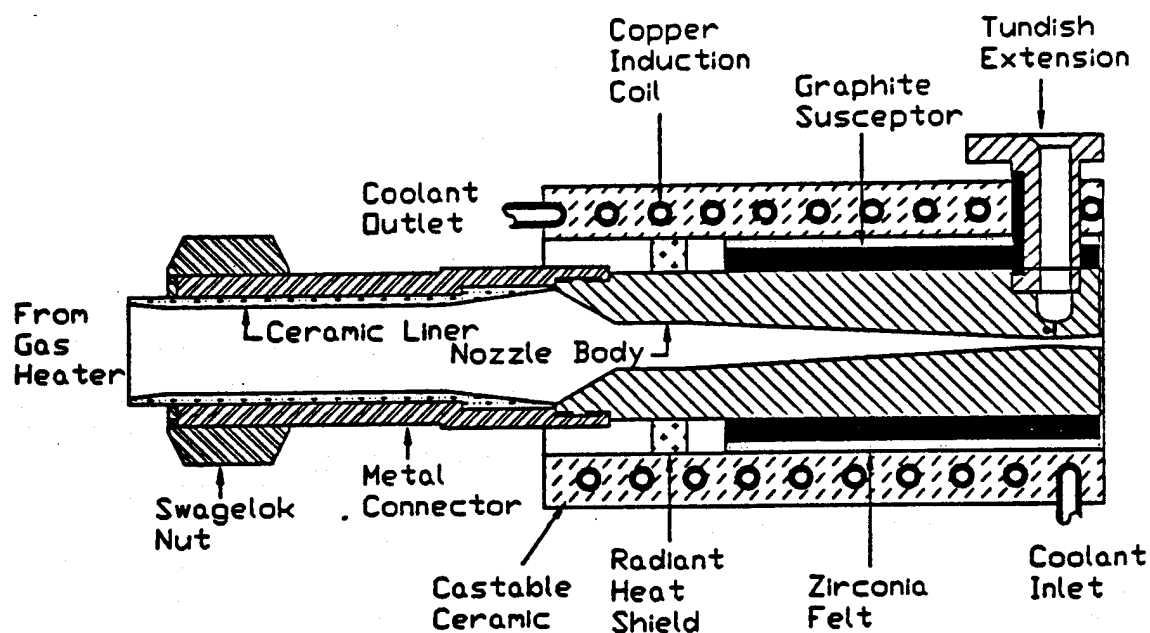A TC entered the nozzle body from one side to sense the combined effects of the inductively-heated nozzle body, resistance-heated gas flowing in the throat, and superheated molten metal poured into the tundish. During latter stages of Phase II, however, the TC hole had to be moved toward the rear, away from the tundish, because molten metal dissolved enough boron nitride to expose the TC junction to direct attack. The only other TC problem was alumina softening near the hot susceptor.

## F. NOZZLE GEOMETRY INVESTIGATIONS

As discussed in the Phase I report (Reference 3), the first phase used a circular nozzle with a single liquid orifice between the tundish and nozzle throat. It was decided to test rectangular nozzles with multiple liquid orifices in Phase II to determine if more uniform coating thickness and minimal edge-tapering could be obtained. Rectangular nozzles would also be more suitable for higher metal deposition rates over larger areas. The goal was to produce uniform coatings at least 1-inch wide at a maximum deposition rate approximately ten times greater than that of the Phase I nozzle.

The rectangular nozzle configuration introduced several effects that had not been observed in earlier tests with tin in multiple-orifice nozzles. In particular, it was found to be quite difficult to initiate and maintain equal aspiration of molten metal through all liquid orifices at the tundish base. Molten tin is evidently much lower in viscosity than the cobalt-chromium alloys tried in Phase II, at least at comparable amounts of superheat.

16

The Phase I nozzle had an entrance cone angle of 38° and an exit cone angle of 10°. The former dimension was established by extensive tin-spraying exercises, while the exit region geometry was optimized by obtaining pressure profiles along the successively trimmed lengths of 6, 10, and 18° nozzles. Similar efforts were required to determine the best entrance and exit angles for Phase II's rectangular nozzles, higher melting point alloys, and higher gas temperatures at the nozzle throat.

Preliminary studies revealed that small-angle entrance contours minimized turbulence in a slot-shaped throat, while small exit angles were best suited for maximum suction across liquid orifices. The 6° entrance and exit contours were selected for Phase II based upon these results.

The nozzles contained a slot-shaped throat and multiple liquid orifices. The gas entrance, throat, and exit regions had rounded corners, a consequence of the tapered tools used for machining. Figure 5, which illustrates the setup for measuring suction among the liquid orifices, shows the exit region and indicates the locations of the orifices. The early Phase II nozzles had six liquid orifices with relatively large
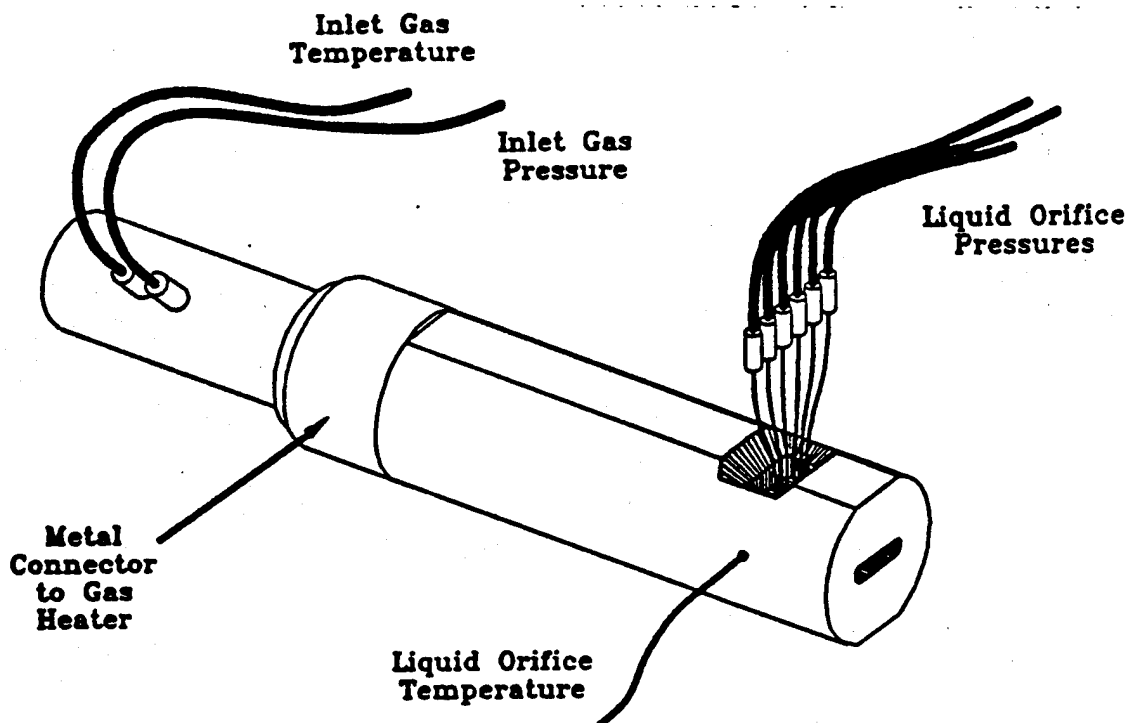


Figure 5. Nozzle Characterization Setup.

17

diameters. However, preliminary spraying trials determined that the liquid streams were not broken up enough for rapid solidification to occur. A 10-hole design, with the orifice diameters reduced to maintain the cross-sectional area, was then adopted. Although the droplet size distribution was greatly improved, the two outermost orifices did not aspirate consistently. This effect appeared to be caused by the proximity of the tundish side walls and the surface tension of the molten metal. The remaining nozzles were fabricated with nine orifices, more side wall clearance, and rounded edges.

At first, the liquid orifices were simply holes drilled directly in the boron nitride at the tundish base. A chamfer at the top of each hole facilitated seating the needles used for suction measurements (Figure 5) and obtaining dependable pressure seals. Once the melt temperature reached 1600°C, however, these holes eroded very rapidly--opening appreciably during a single 30-second spraying experiment. Larger holes were then drilled in the boron nitride to accommodate alumina tubes, which were held in place by ceramic glue. With the alumina inserts the service life of a nozzle was generally limited by melt dissolution or erosion of boron nitride at the tundish base that resulted in loss of the alumina inserts or, in more severe situations, collapse of the entire tundish base into the throat.

At typical nozzle and melt temperatures of 1600 to 1700°C, respectively, a nozzle could sustain four to five spraying trials before erosion of the boron nitride tundish base (surrounding the orifice tubes) became prohibitive. This area eroded slightly faster at higher operating temperatures, but at least three spraying trials could be expected at temperatures up to 1900°C. Another nozzle deterioration mechanism became dominant as operating temperatures approached 2000°C, the temperature required for spraying molten chromium. Since nozzle temperature was measured near the throat, which was cooled by the flowing nebulizing gas, temperatures were significantly higher at the nozzle periphery, adjacent to the graphite susceptor. At elevated peripheral temperatures, the graphite and boron nitride would react to form boron carbide and nitrogen gas. This

phenomenon proceeded gradually during the experiments with cobalt-chromium alloys, and the only noticeable effect was a slow loss in susceptor material and a net decrease in heat transfer to the nozzle body, which did not impact the nozzle service life as much as tundish erosion did. However, the nozzle-susceptor reaction did effectively preclude spraying pure chromium. As discussed previously, sufficient molten boron carbide formed to melt through the nozzle sidewalls and plug the exit region during the pure chromium trial, even with a fresh nozzle and susceptor.

The nozzle operating pressure as the furnace charge was poured into the tundish was a related problem. During Phase I, the preferred method was pouring while a slight overpressure existed in the throat, such that a small amount of argon gently bubbled up through the single liquid orifice into the tundish. Unfortunately, small variations in suction among the multiple orifices (attributable to boron nitride flaws or machining defects) prevented this technique from succeeding in Phase II. Preventing all of the liquid orifices from aspirating until desired created excessive overpressure at some orifices, resulting in vigorous tundish agitation and occasional melt ejection. Pouring at aspirating pressures did not work either--molten metal would often be aspirated only through the first orifices reached. The extra gas flow underneath the remaining orifices created local overpressures and prevented subsequent aspiration through them. This allowed the gas to go around the incoming liquid streams, rather than efficiently shearing them into fine droplets. Consequently, molten metal dribbled along the nozzle roof, eroding conspicuous grooves in the boron nitride in the process.

After considerable trial and error, the technique adopted for much of Phase II was pouring with no gas flow through the nozzle. The gas heater was first brought to equilibrium conditions at approximate spraying flows, whereupon the heater was turned off and the nebulizing gas valve was closed to prevent loss of heat stored in the gas heater. Then the furnace charge was poured. No molten metal flowed into the nozzle throat at this time because surface tension prevented it from entering the small holes. Only when gas flow was restarted (followed immediately by switching on the gas

heater) was sufficient suction present at the liquid orifices to break the surface tension and commence aspiration. This approach brought molten metal into contact with all liquid orifices before beginning the argon flow, so that strong aspiration through all orifices occurred.

While the above technique worked adequately with the iron-element gas heater, it was not well suited for the tungsten-element heater employed toward the end of Phase II. Even without gas flowing through the heater, the tungsten elements would have cooled substantially during the pouring operation and the corresponding decrease in resistivity would cause a major current surge, and probably element damage, when power was switched on unless the voltage settings on the variable transformers were decreased. Consequently, gas flow and power were maintained, and pouring was performed at spraying pressures inside the nozzle throat.

## G. BASE METAL FIXTURING

Two base metal fixtures were used to move the coupons during Phase II. A rotating drum arrangement was employed for the initial spraying trials with the cobalt-chromium alloys which produced no adherent coatings. This fixture consisted of a three-jaw chuck coupled by gears to a fixed-speed drive motor. As such, it was very similar to the fixture used for much of Phase I (Figure 23 of Reference 3). The major differences in Phase II were the lack of a variable-speed drive motor and the absence of a thick aluminum drum to support the thin base metal sleeves. For Phase II, relatively thick (0.060 and 0.080 inch) self-supporting stainless steel cylinders were mounted directly on the chuck. Without preheating, the cylinders were evidently too much of a heat sink for effective consolidation of droplets at the base metal surface.

The vertically-oriented fixture with which all the successfully coated coupons were produced in Phase II is displayed in Figure 6. This fixture resembles the one used near the end of Phase I, with several refinements. The vertical drive now used a direct rack and pinion system, instead of a light-weight cable. With a high torque motor, the drive system accelerated
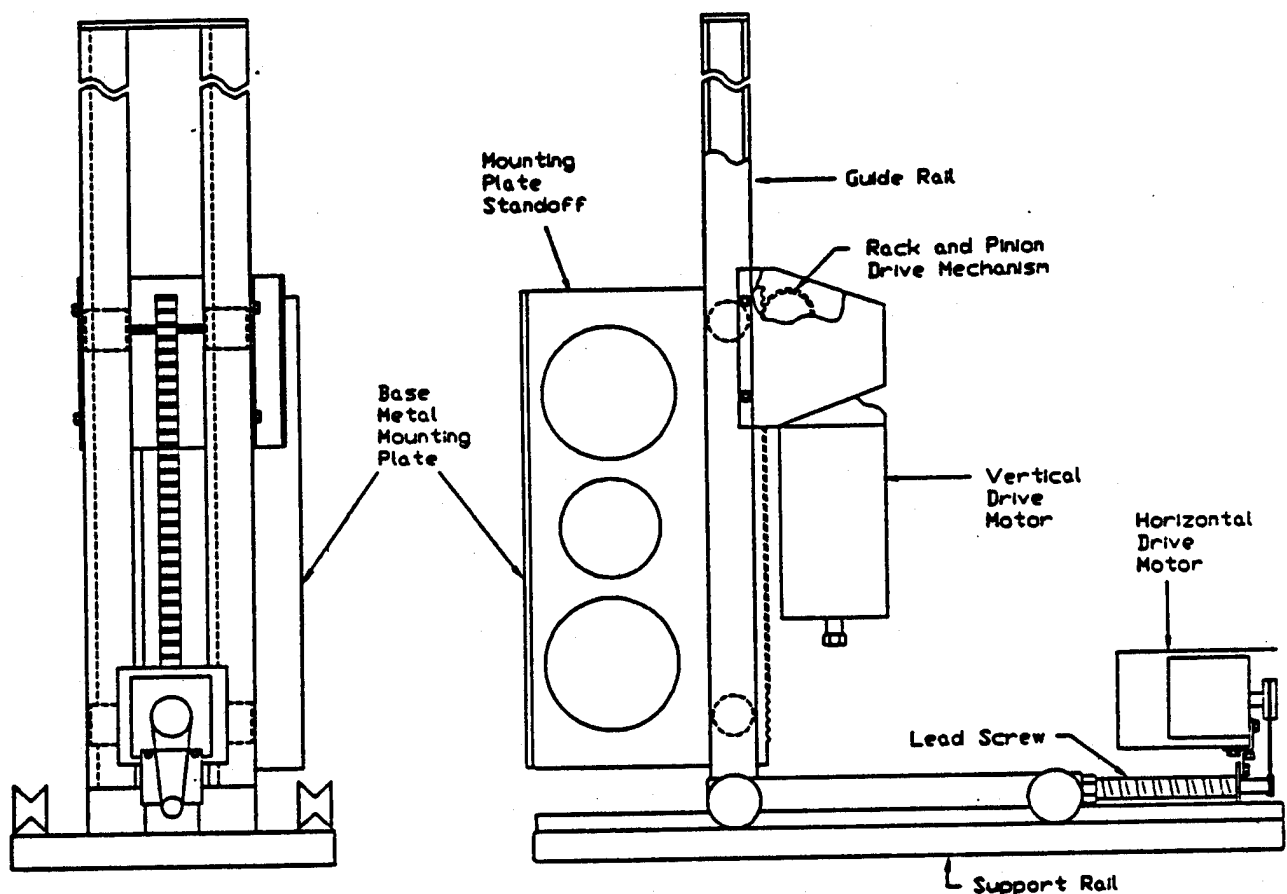
Figure 6.  Back and Side Views of Vertical Base Metal Translator.

the base metal to the desired speed almost instantly.  The speed signal recorded by the computer was taken from the potentiometer in the remote speed control.  Because of the high motor torque and the rack and pinion system, this signal more accurately represented actual base metal speed than the signal from the Phase I system did.

The Phase II vertical fixture used coupons approximately 1-inch wide and 0.035-inch thick by 20- to 22-inch long.  Each strip was spring-clamped to the mounting plate.  In the Phase I fixture, the coupon was prone to bowing under pressure from the nozzle plume, unless it was counterbalanced by a preheating flow directed against the back side.  The addition of a large standoff between the guide rails and the mounting plate for Phase II primarily protected the drive motor from hot nozzle gas.  However, it also permited attaching a wide mounting plate, which both supported the coupon

21

and also allowed considerable flexibility in base metal placement and strip width.

Unlike Phase I, a dedicated base metal preheater was not used in this phase. Deposit adhesion might have been promoted at slightly lower furnace and nozzle temperatures by employing a separate preheater for the base metal strips. However, with the much higher gas temperatures exiting the nozzle in Phase II, merely placing a thin (0.035-inch) base metal coupon in front of the nozzle 4 inches from the liquid orifices allowed the base metal temperature to approach 200°C. Auxiliary preheating was not considered to be necessary under these circumstances, although it would probably be desirable for thicker base metals. Sophisticated monitoring of base metal temperature was also unnecessary. One spring-loaded thermocouple was placed against the front surface of the coupon immediately below the spray elevation. This was adequate for measuring the temperature of the first base metal portion to be contacted by droplets.

The base metal's position in front of the spray plume affected many coating characteristics. Nebulizer-to-base metal distance governed the extent of mixing between hot gas leaving the nozzle and cool chamber gas, the amount of droplet deceleration during the mixing process, and, along with the plume expansion angle, the plume width upon reaching the base metal. Consequently, this distance influenced droplet temperature at impact, heat flux available to support consolidation, and convective gas cooling after deposition. Coating thickness was also affected by the speed of translation across the spray plume.

The nozzle-to-base metal distance was adjusted remotely, and the base metal was normally positioned 4.0 to 4.5 inches from the liquid orifice. Consolidation behavior was estimated visually, with the objective of maintaining one-fourth to one-half of the deposition surface in a shiny molten condition, depending on metal spraying rates.
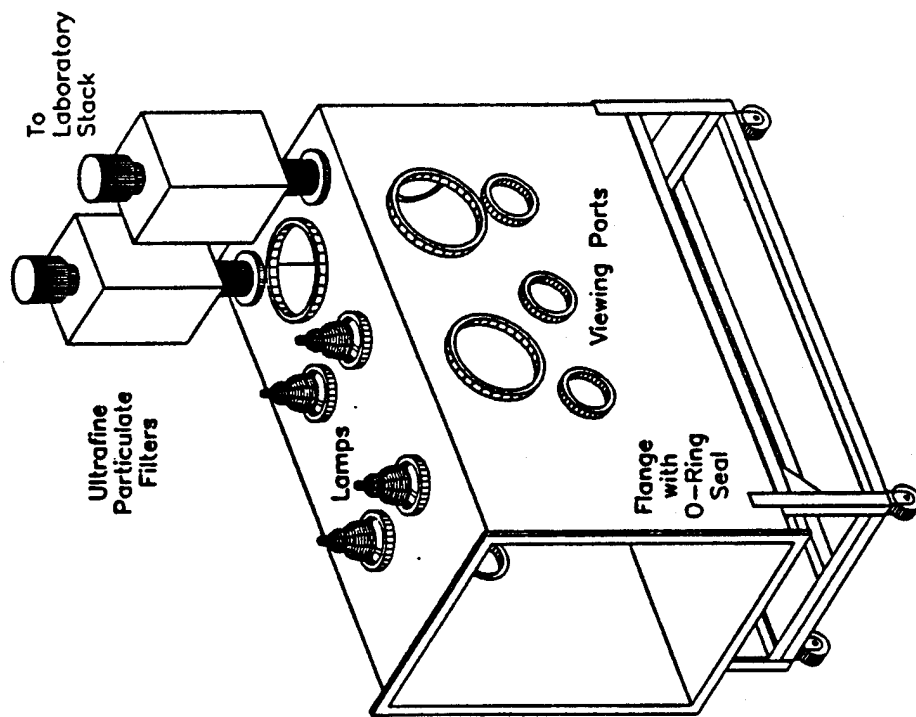
## H. SPRAY SYSTEM ISOLATION CHAMBER

The main purposes for the spray system isolation chamber were to protect laboratory personnel from all potentially dangerous experimental situations, to limit gaseous reactions with molten metal droplets and hot components, and to filter out all metal particles before discharging the chamber atmosphere to the environment. All of these goals were met with ample margin at low cost by the chamber shown in Figure 7. Controlled environments would probably be used in commercial spray coating. In large-scale use, economic benefit could be derived from recycling the nebulizing gas and any unconsolidated metal powder (overspray).

The chamber housing, rolled back from the experiment platform, is shown in Figure 1. All of the penetrations for inert nebulizing and purging gas, thermocouple feedthroughs, pressure transducer lines, gas heater power leads, induction power, and coolant flow were on the side of the chamber that was fixed to the experiment platform so that the chamber could be opened and closed without disturbing any of these critical connections. Although both the experiment platform and the chamber housing were mounted on rollers, only the main housing was moved in actual practice. All components of the spray system were operated remotely, eliminating possibilities for directly contacting molten metal, hot components, and exposed electrical leads. The O-ring seals on the chamber ports and main flange prevented escape of metal particles and enabled purging to oxygen levels of less than 1 percent.

Purge gas lines entered near the top and bottom of the chamber to sweep it free of oxygen and other reactive gases, while purge lines near the middle cooled the motors for the base metal translator and furnace tilting mechanism, along with the internal cable tray. The argon purge flow (~50 scfm) was maintained for 15 minutes before component heatup was begun in preparation for a spraying trial. This purging rate was held throughout the heatup sequence and spraying activities, as well as during cooldown, to prevent oxidation of the graphite susceptors. This procedure was sufficient to prevent any in-flight oxidation of droplets, since no oxide

Thermocouple
Feedthroughs

Nozzle
Supply

Gas Heater
Power

Pressure
Transducer
Lines

Induction Supply
Power/Cooling

Chamber
Purge

b) Gas and electrical penetrations permanently
attached to experiment platform)

To
Laboratory
Stack

Ultrafine
Particulate
Filters

Lamps

Flange
with
O-Ring
Seal

Viewing Ports

a)  Housing and particulate filters

Figure 7.  Spray System Isolation Chamber.

24

inclusions were detected at splat boundaries during metallographic examinations of coating samples. More expensive evacuation and backfill approaches were thus found to be unnecessary, and standard motors could also be used on the furnace tilt mechanism and on the base metal fixture.

The chamber housing had two Flanders Airpure high efficiency particulate filters designed to remove all particles larger than 0.3 micrometer in diameter from the exhaust flow. One filter led to the laboratory stack exhaust, the other was attached to a membrane-covered opening that was a pressure-relief valve for the very unlikely event of a blockage in the stack filter.

Particle size and concentration were measured within the spray chamber and within the filtered exhaust stream by two LAS 250X laser aerosol spectrometers (Particle Measurement Systems, Inc.). These spectrometers contained a small pump that extracted 0.01 of the exhaust volume for continuous analysis; the pump throughput and sample line diameter were carefully set to extract gas at the same velocity as it flowed through the main duct. This "isokinetic" method assured that all samples were representative. Auxiliary cooling was required to bring the exhaust gas temperature below 30°C whenever particulate measurements were made, because the aerosol spectrometers could be damaged by higher sampling temperatures. Liquid argon, fed through a coil of copper tubing suspended in the chamber near the exhaust port, cooled the exhaust flow for sampling.

Each spectrometer segregated incoming particles into 16 size ranges according to scattered light intensity (size ranges were calibrated periodically with appropriate aerosol standards). Particles in all 16 channels were counted for a preselected interval, typically 30 seconds, and the tallies sent to a computer for later data reduction. Aerosol spectrometer measurements downstream of the ultrafine particle (0.3-micrometer) filter were not able to detect any increase above background in exhaust emissions when spraying.

Difficulties were experienced in achieving stable nozzle operation for a sufficiently long time to produce an equilibrium concentration of tiny "overspray" droplets inside the chamber, which generally result from splashing of incident droplets on the deposition surface. However, a worst-case analysis concluded that maximum concentrations would be at least three orders of magnitude below the threshold for pyrophoric hazards, in the event of a sudden accidental ingress of oxygen (such as by catastrophic failure of a chamber port).

# SECTION III
## SPRAY COATING EXPERIMENTS

## A. INTRODUCTION

The plan for the Phase II feasibility study was that once the spray system components had been designed, tested, and assembled, an initial set of steel specimens would be coated with high melting point material over wide ranges of operating parameters. The coating quality of these samples was then to be evaluated. Based upon these results, a second set of specimens would be coated at spraying conditions likely to yield coatings with good adhesion, porosity, hardness, etc. Finally, a third series of experiments would be performed to optimize overall coating quality. This task sequence was based upon the assumption that all major components of the spray coating system would function as desired without modification. Unfortunately this was not true. Numerous alterations had to be made to the nebulizing gas heater over the course of Phase II, as already discussed, and only near the end were the desired argon temperatures produced at the nozzle inlet. Consequently, gas temperature could not be varied across the range necessary for comprehensive experiments until quite late in Phase II. Spray system development required important aspects of the equipment and operations to be changed on several occasions; therefore, a rigid test matrix was not followed. However, this did not prevent achieving the goal of Phase II, demonstrating that coatings of good quality can be sprayed from high melting point materials.

## B. MATERIALS

The spray coating process being developed is intended to replace electroplating chromium. However, a tremendous gap exists between the melting point of the tin used in Phase I (232°C) and that of elemental chromium (1857°C). Instead of attempting so massive an increase in operating temperatures in one step, it was deemed wiser to first spray cobalt-based alloys of high chromium content with melting points in the

27

neighborhood of 1370°C. Cobalt-chromium alloys, such as Stellite 6, have traditionally been used for "hardfacing" applications that demand a combination of wear and corrosion resistance. Due in part to the presence of dispersed carbides, such alloys may outperform chromium. Deferring attempts to spray pure chromium until the latter stages of Phase II also helped to accommodate the long procurement lead times and fabrication delays at GTE Sylvania in building the custom tungsten elements for the gas heater, which were essential to experiments on molten chromium.

Three cobalt-chromium alloys were sprayed in this investigation. Stellite 6 and Haynes Ultimet were selected because they were developed for wear resistance and galling resistance, respectively. Another wear-resistant alloy, Coast 64, was added at the recommendation of Tinker Air Force Base. The compositions of these alloys are, in weight percent,

|  | Chromium | Nickel | Molybdenum | Tungsten | Carbon | Cobalt |
|---|---|---|---|---|---|---|
| Stellite 6 | 27 | | | 4 | 1 | Bal |
| Ultimet | 27 | 9 | 5 | | 0 | Bal |
| Coast 64 | 27 | 4 | | 19 | 1 | Bal |

Stainless steel coupons were used for the first few trials, but low-carbon steel (ASTM A366, AISI 1010) was used exclusively afterwards since most components refurbished at Tinker Air Force Base are fabricated from 4340 deep-hardened low-carbon steel. Surface preparation consisted of grit-blasting with coarse Number 30 alundum. Base metal strips were nominally 20- to 22-inches long and 1-inch wide. The length was fixed by the extent of travel on the translation fixture, while the width was chosen to accommodate lateral plume expansion from the 0.75-inch wide throat over the 4-inch separation distance.

## C. COATINGS

The coating experiments were named according to the date on which they were performed. For example, the first successful coating experiment, performed on October 5, 1990, was termed the J2780 experiment, because

28

October 5 was the 278th day of the year and 0 is the last digit of the year. When more than one experiment was performed on a given day, a sequence number was added (-1, -2 etc.). The spray system configuration and parameters for the coating experiments are listed in Tables 1 and 2, respectively. Typical coatings of the three materials are described below.

A cross section of a Coast 64 coating (J3100-2) is shown in Figure 8. The deposit, a combination of irregular, multiple passes, was uniformly thin, with a glassy microstructure and occasional tiny bare areas. The microstructure is either amorphous or nanocrystalline (X-ray diffraction could not be performed on such a thin a layer). The main features of this sample are: (1) splats that consolidated quite well in most places, including at the interface, in spite of very fast solidification (the splats were probably highly undercooled, not just incident droplets); and (2) brittle fracturing from residual stress in the warped base metal, which attempted to straighten during cooling. In Figure 8, Area A shows fracturing along the splat interface region; the fine features could be microvoids. Area B is a thin region with cracking around a large droplet. There were also different size droplets that nearly solidified in flight. Area C delaminated from the base metal and exhibited unusually poor splat consolidation for this sample. Area D revealed good mechanical bonding, except for the entrapped gas bubble.

Stellite 6 deposits are shown in Figures 9 (J3130) and 10 (J3190). J3130 produced a thin, shinny coating that was near molten when deposited. The splats are very large, possibly indicating dribbling along the roof, which would also explain the large entrapped gas pore. The microstructure is fine dendrites. Splat boundaries etched differently than interiors, which suggests that the droplet (or globule) surfaces were solidified before impact. High heat flux is suggested by the growth of fine dendrites across the splats. In Figure 9, Area A reveals a small, uniform matrix structure. Area B is a molten deposit containing carbon-rich bands. Area C contains the same wavelike ridges of carbon-rich bands that are darker in color, with unusually low hardness measurements in the boundaries. Coating J3190 was sprayed at a cooler temperature than J3130,

29

Table 1. Spray system configuration for coating experiments

| Coating number | Material and amount sprayed (g) | Base metal[a] | Gas heater element | Nozzle material | Nozzle configuration | Orifice size (in.) | Nozzle ID |
|---|---|---|---|---|---|---|---|
| J2780 | Haynes Ultimet, 75 | SS | Iron | Union Carbide HBC grade | 6/6 degree, 10-holes | 0.016 ID | DN2710AC |
| J3100-2 | Coast 64, 49.8 | SS | Iron | Combat AX05 | 6/6 degree, 10-holes | w/Al$_2$O$_3$ tube, 0.016 ID | DN3050AC |
| J3130 | Stellite 6, 55.5 | CS | Iron | Union Carbide HBC grade | 6/6 degree, 10-holes | w/Al$_2$O$_3$ tube, 0.016 ID | DN2980AC |
| J3190 | Stellite 6, 56 | CS | Iron | Combat AX05 | 6/6 degree, 9-holes | w/Al$_2$O$_3$ tube, 0.020 ID | DN3190AC |
| J3320-1 | Haynes Ultimet, 48.6 | CS | Iron | Combat AX05 | 6/6 degree, 9-holes | w/Al$_2$O$_3$ tube, 0.020 ID | DN3300AC |
| J3330 | Coast 64, 50.1 | CS | Iron | Combat AX05 | 6/6 degree, 9-holes | w/Al$_2$O$_3$ tube, 0.020 ID | DN3300AC |
| J3370-1 | Stellite 6, 45.7 | CS | Iron | Combat AX05 | 6/6 degree, 9-holes | w/Al$_2$O$_3$ tube, 0.020 ID | DN3300AC |
| J3370-2 | Coast 64, 51.4 | CS | Iron | Combat AX05 | 6/6 degree, 9-holes | w/Al$_2$O$_3$ tube, 0.020 ID | DN3300AC |
| J0041 | Stellite 6, 45.3 | CS | Tungsten | Combat AX05 | 6/6 degree, 9-holes | w/Al$_2$O$_3$ tube, 0.020 ID | DN3590AC |
| J0601 | Pure chromium[b] | CS | Tungsten | Combat AX05 | 10/6 degree, 9-holes | w/Al$_2$O$_3$ tube, 0.020 ID | DN3550AC |

a. SS - stainless steel, CS - low carbon steel
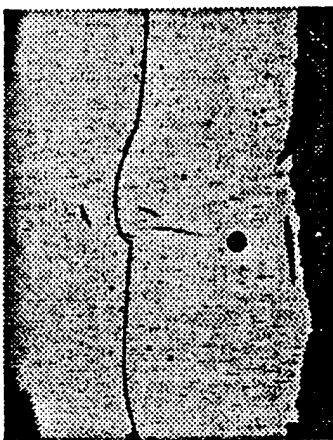b. Melted but not sprayed due to nozzle-susceptor reaction

Table 2. Spray system parameters for coating experiments

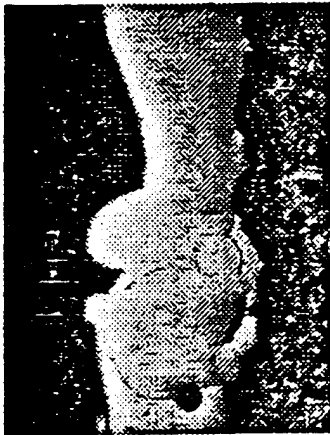| Sample Number | Temperature (°C) | | | Argon aspirating gas pressure (psi) |
| --- | --- | --- | --- | --- |
| | Furnace | Nozzle | Gas outlet | |
| J2780 | 1550 | 1630 | 600 | 19-22 |
| J3100-2 | 1650 | 1580 | 600 | 19-23 |
| J3130 | 1850 | 1550-1600 | 610 | 18-21 |
| J3190 | 1700 | 1640 | 550-620 | 18-21 |
| J3320-1 | 1780 | 1700 | 620 | 19-25 |
| J3330 | 1850 | 1620 | 620 | 19-22 |
| J3370-1 | 1890 | 1760 | 730 | 19-21 |
| J3370-2 | 1870 | 1740 | 730 | 20-30 |
| J0041 | ~1900 | 1700 | 1140 | 18-30 |
| J0601[a] | ~2100 | 2000 | ~1100 | ~21 |

a. Melted but not sprayed due to nozzle-susceptor reaction

and its splats are much smaller and the deposit is both wider and more symmetric, indicating that the melt aspirated through all the liquid orifices with much better breakup and that there was no dripping along the roof. For this specimen, the base metal warped because there was more heat at the crown than there was at the edges. However, the mechanical bonding was so good that no delamination occurred. Very rapid solidification is indicated by the porosity from incomplete droplet consolidation (lenticular pores, instead of round ones from entrapped gas). Only one brittle fracture occurred in J3190 (Area C), unlike earlier Coast 64 coatings. Figure 11 presents optical and SEM (opposite orientations or mirror images) micrographs of J3190 in the area of cracking. Splat boundaries were highlighted by a cathodic etch, using a strong oxalic acid. Carbides

Area A - Cracking along splat interface

Area B - Thin region with cracking around droplet

Specimen support spring

25 μm

25 μm

32

Area C - Delamination

50 μm

Area D - Mechanical bonding.

25 μm
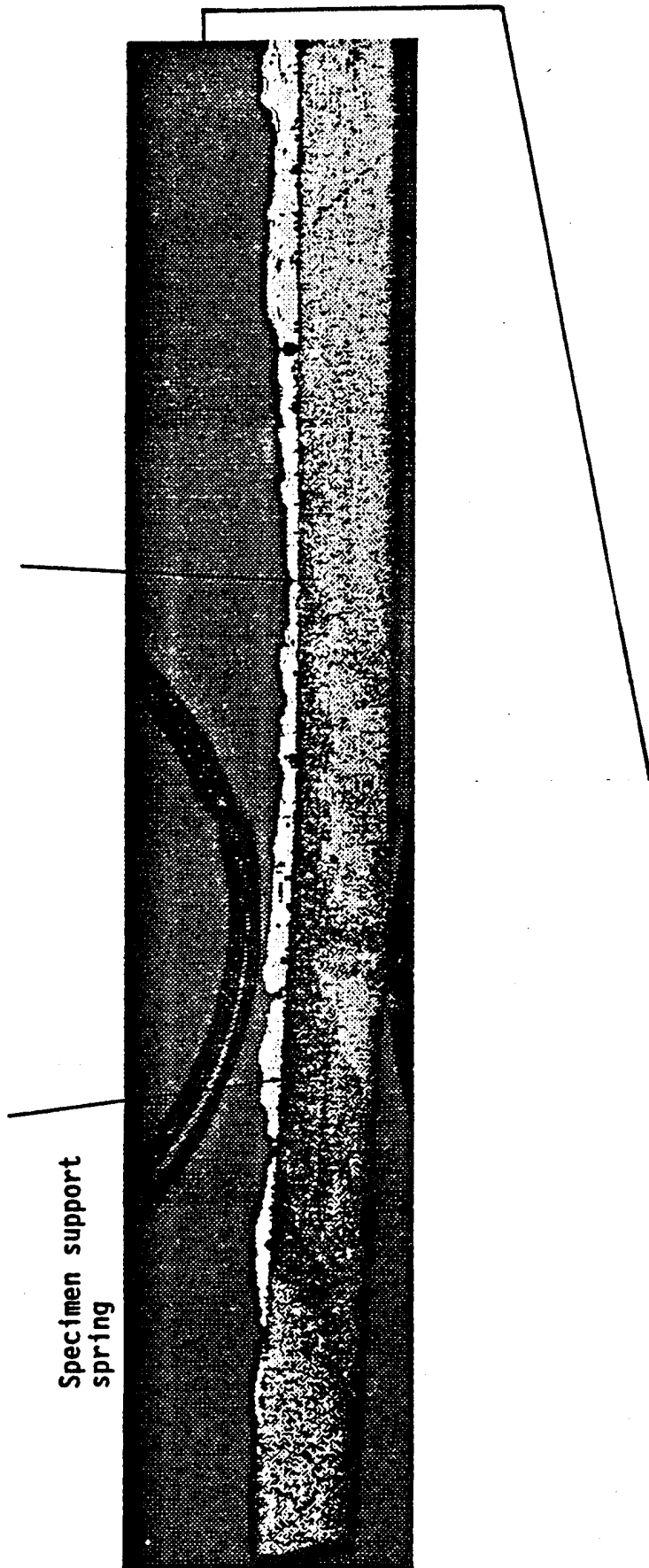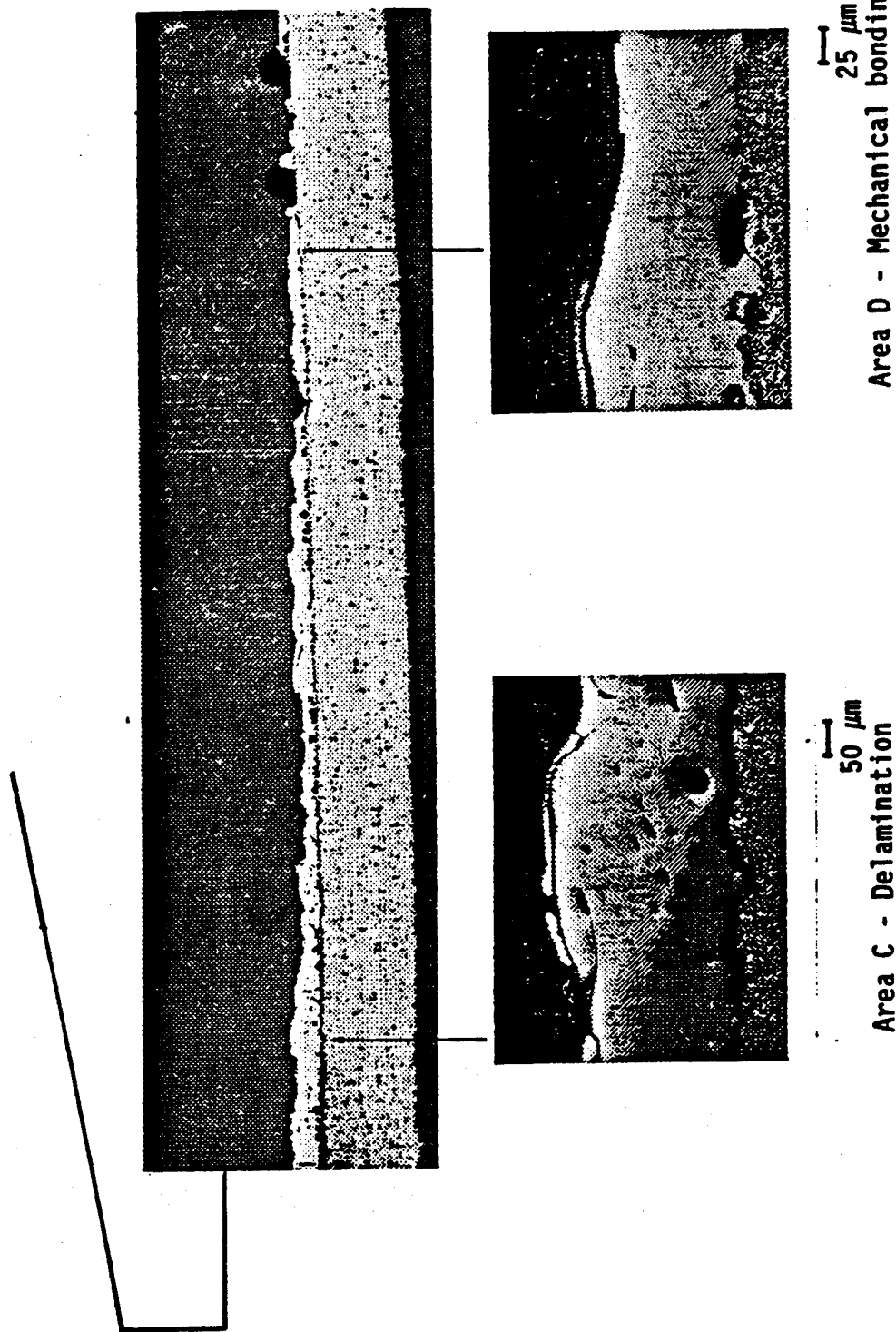
Figure 8. Coast 64 Deposit (J3100-2, Sample M-3).

33

100 μm

Area C - Wavelike ridges of carbon-rich bands

50 μm

Area B - Molten deposit containing carbon-rich bands

25 μm

Area A - Small, uniform matrix

Entrapped gas pore
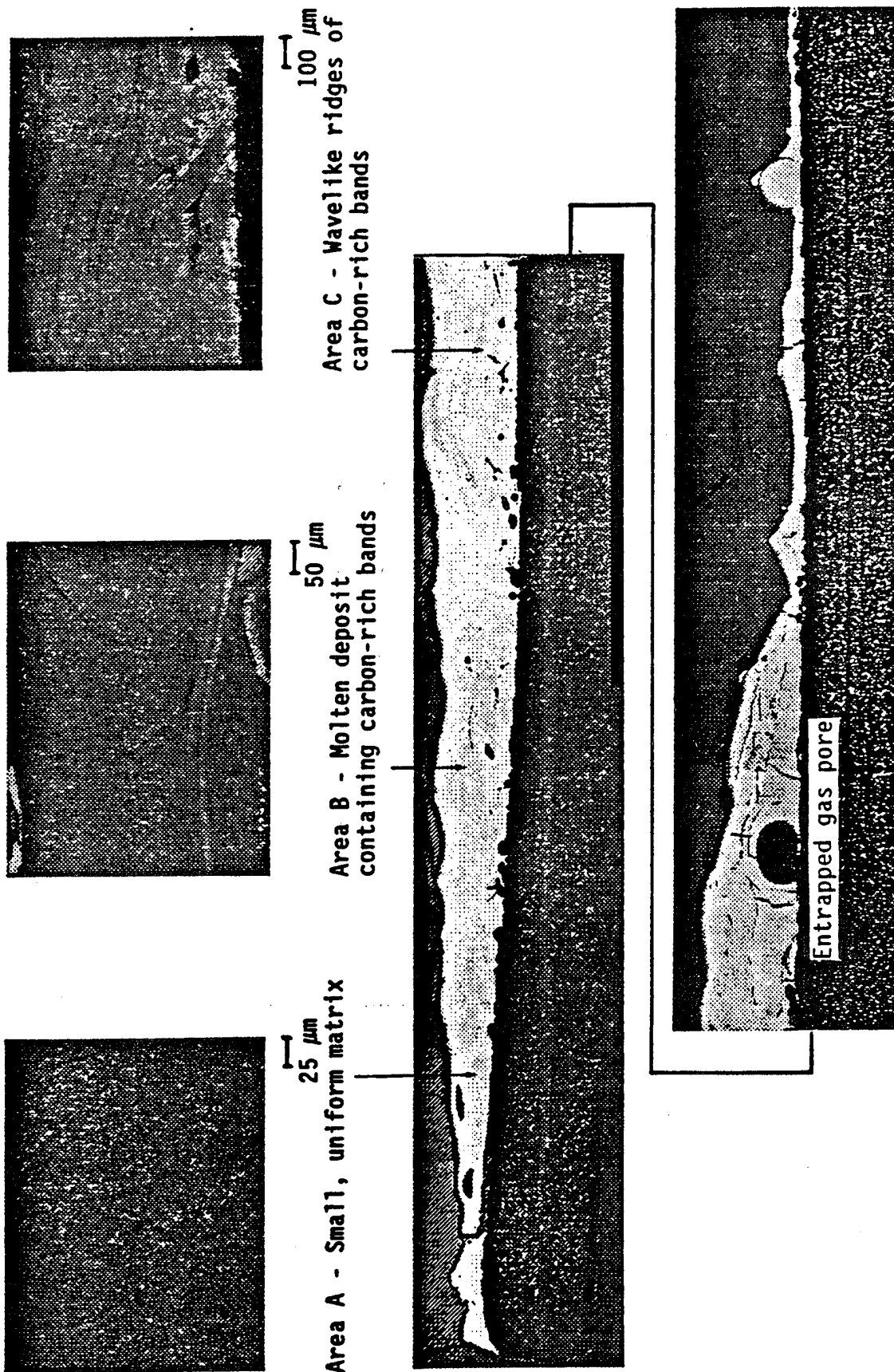
Figure 9. Stellite 6 Deposit (J3130-2, Sample M-2).

50 µm
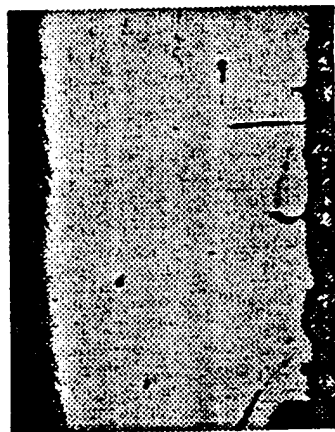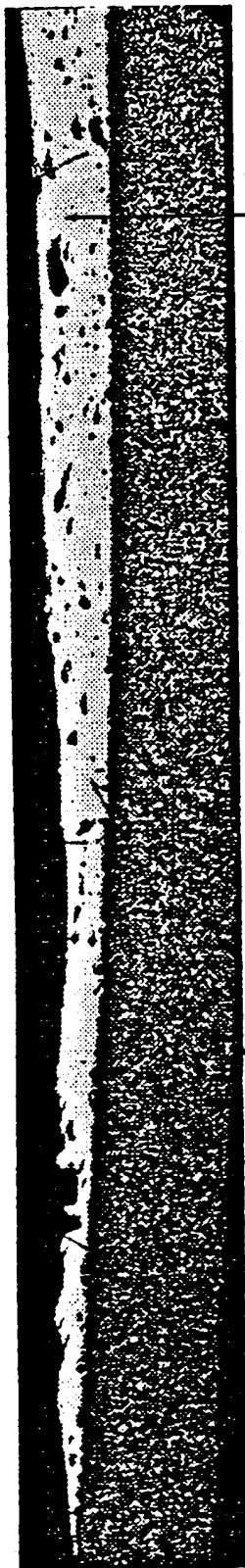
Area C - Brittle fracture
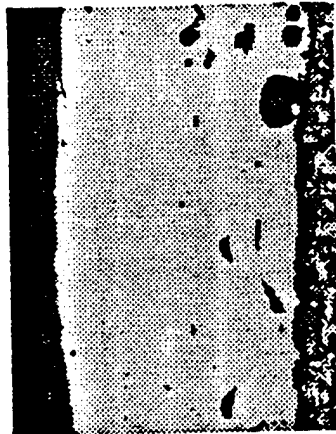
Area B - 6% bulk porosity

50 µm

50 µm

Area A - Low porosity
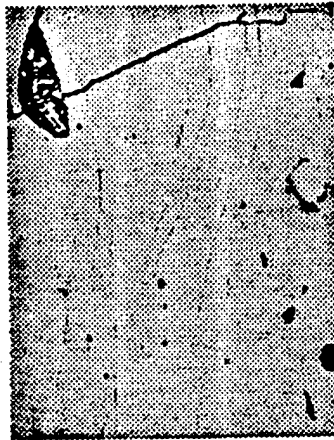
Area shown in Figure 11.

Figure 10.  Stellite 6 Deposit (J3190-2, Sample M-2).
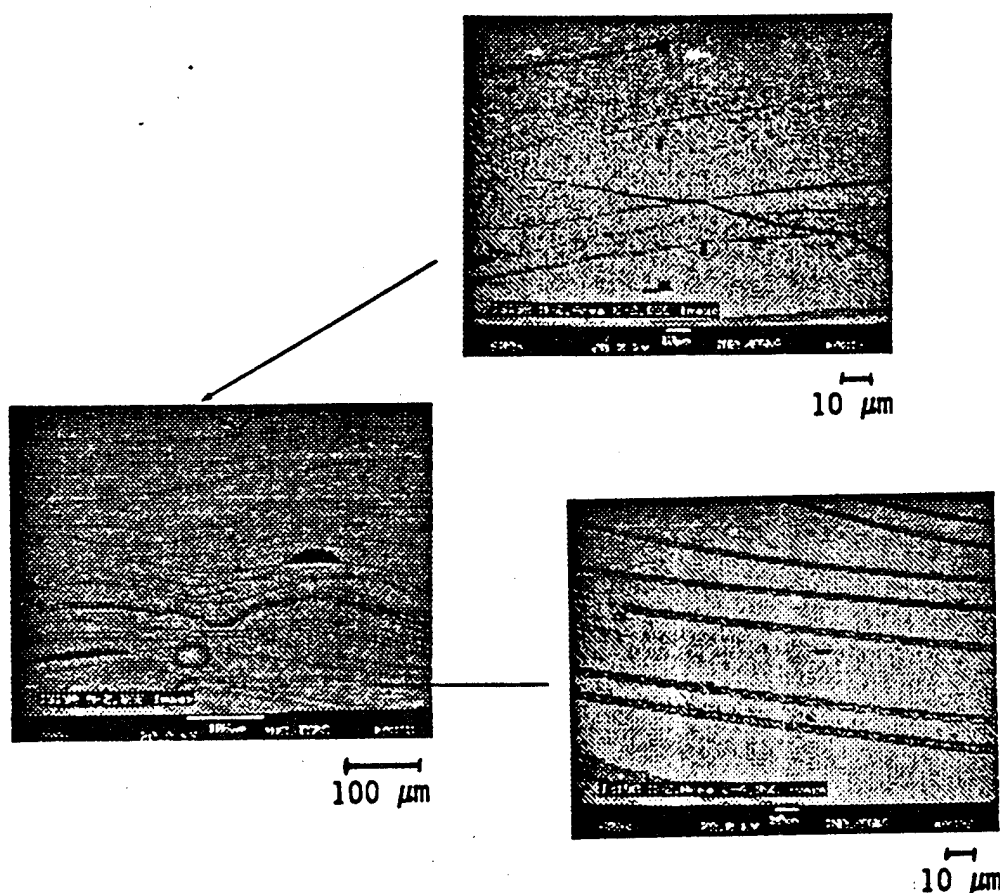
Figure 11.  Region of Horizontal Cracking from Figure 10.

smaller than 1 $\mu$m are found at 5000X.  Areas of extensive brittle cracking
are shown.

The first successful coating, a Haynes Ultimet deposit, was produced in
J2780.  The thick coating was formed from large molten globules, caused
when the boron nitride liquid orifices eroded.  The large, rounded pores
are attributed to gas entrapped by irregular melt globules that probably
dribbled along the nozzle roof.  There was little interfacial porosity
under the thick crowns.  There was no bonding at the edges, where the
deposit warped away from stainless steel base metal due to differential
thermal contraction.  The microstructure exhibited equiaxed grains or
columnar dendrites, where the large heat flux caused grain growth across
the splat boundaries or where all splats consolidated while fully liquid.
Another Haynes Ultimet coating, J3320-1, is shown in Figure 12.  Experiment
J3320-1 was conducted at much lower temperatures than J2780.  The

Specimen support spring
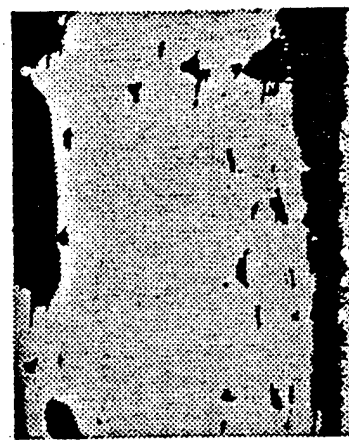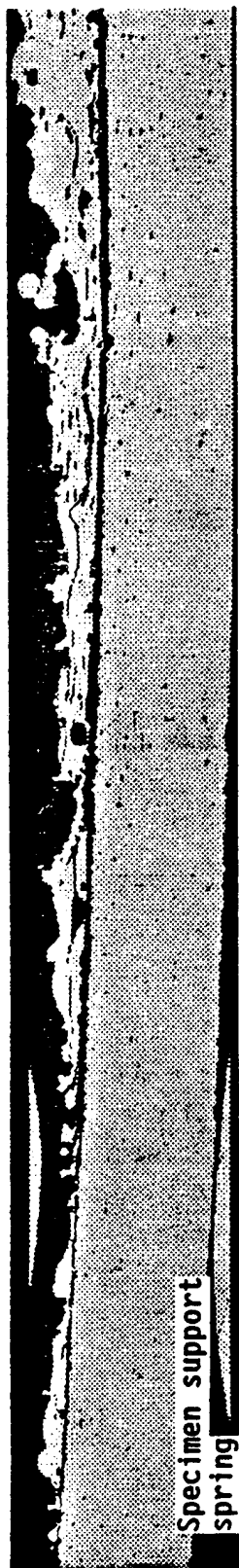
Area A - 2.8% bulk porosity

Area B - Dendrites larger near exterior than substrate
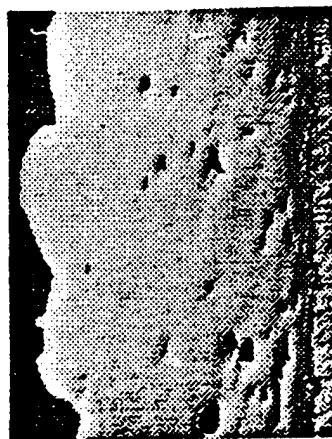
Area C - Mechanical bonding

Figure 12. Ultimet Deposit (J3320-1, Sample M-1).

37

microstructure was dendritic, and there was a great deal of porosity from incomplete splat consolidation. The deposit was thicker on the right side of the base metal due to mispositioning of the strip and to biased spraying from the nozzle. It appears that the middle of the deposit warped away from the base metal, rather than the base metal warping away from the deposit as in other experiments. Area B shows larger dendrites at the coating exterior than at the base metal, probably due to slower heat transfer.

## D. SAMPLE ANALYSES

The attributes of coating quality measured during Phase II were porosity, hardness, and adhesion to the base metal.

### 1. Porosity

Porosity formed either from incomplete droplet consolidation or from gas entrapment in near-molten layers. Percent porosity was measured on photomicrographs of areas of interest using a Baush and Lomb Omni Con Alpha Image Analysis System. The results of these measurements are shown in Figure 13. All plotted values are area averages within the coating layer, i.e., open areas on the surface and delaminated regions were excluded. The porosity was never interconnected.

No statistically-significant differences were found among the three cobalt-chromium alloys, which is not surprising in light of their similar compositions. Droplet consolidation is strongly influenced by the thermal and fluid properties of impacting droplets, and similar compositions should consolidate to a similar extent, assuming uniform deposition conditions.

No clear differences in porosity were found among the various experiments conducted with each alloy, although the spraying conditions were quite distinct in certain cases. This is because 1) these measurements did not discriminate between porosity due to incomplete consolidation at lower deposition temperatures, and gas entrapment, which
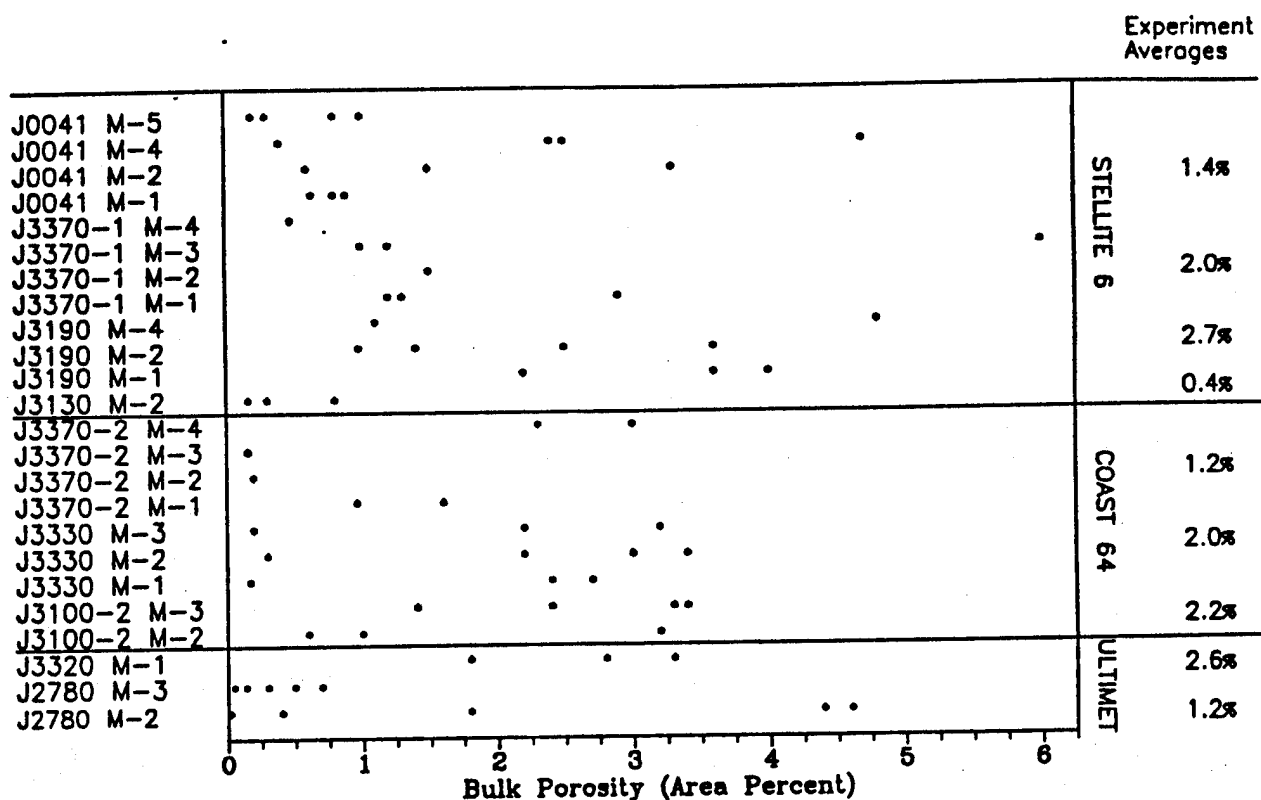
Figure 13.  Coating Porosity.

was more common with higher heat fluxes; and 2) porosity varied appreciably among samples from a given experiment, as well as among areas within a single sample, due to variations in coating thickness and local heat flux.

The results suggest that bulk porosity was a stochastic variable during Phase II, where local porosity levels could be expected to vary between 0 and 5%.  This spread in porosity levels partially reflects the random locations and timing of droplet impact, which caused certain areas to always be deprived of sufficient mass and thermal flux to foster complete splat consolidation.  However, Phase II porosity values were also deterministic, in that nebulization behavior has a critical influence. Recall that much difficulty was encountered in achieving equal aspiration among the liquid orifices, whereupon the diversion of nebulizing gas around the incoming melt streams caused variable droplet shearing.  The droplets sprayed were thus larger than desired and more coarsely distributed.  A larger number of smaller droplets would likely have produced more uniform coatings, although deposition would still have been a random process.

Unequal aspiration also affected formation of porosity from gas entrapment. In certain of the experiments, especially those at higher temperatures, melt streams were not always drawn into the throat with adequate suction to reach the center of the gas stream, resulting in dribbling along the nozzle roof. This poorly nebulized material evidently dislodged from the roof in sheets, rather than droplets. It appeared that such sheets tend to tumble in the gas plume, often wrapping around gas to form a large hollow droplet. However, direct diagnostic measurements of the spray plume were beyond the scope of Phase II.

Despite the possibilities for improvement, it should still be recognized that the Phase II porosity levels were quite good. The porosity was not interconnected (interconnection diminishes corrosion resistance). Furthermore, values near two area percent are better than what is normally achieved with other coating techniques, such as plasma spraying and arc spraying. Thirdly, levels near five percent are common without special modifications, such as spraying in a vacuum (Reference 4). The Phase II results are poor only when compared to the one percent average levels achieved in Phase I.

Six anomalously high porosity values (not included in Figure 13) were obtained at locations of brittle fractures. Small segments of coating would occasionally break free during rough grinding of the metallographic samples. These areas and cracks, which together comprised from 7.3 to 33.5 area percent of the coatings, were not indicative of porosity from either incomplete consolidation or gas entrapment. However, they do reflect the brittle nature of the rapidly solidified cobalt-chromium alloys and could pose a problem in actual components.

The brittle fractures were most likely due to differential thermal stress, which could arise from two primary sources. First, the Gaussian distribution of mass and heat in the plume generally heated the center of the base metal strips more than the edges and tended to warp the thin strips in the transverse direction during deposition, particularly where coatings were thicker. After cooling, residual stresses in the base metal

were prevented from relaxing by the stiff, mechanically bound coatings. Differential contraction, due both to a mismatch in thermal contraction coefficients between the coating and the base metal and to coatings being initially warmer than the base metal, also contributes to stress. Cracks formed and propagated in thicker, brittle coatings where stresses were highly concentrated during cooldown and during sample sectioning and grinding. However, crack formation was rare in thinner coatings closer to the 0.010-inch target thickness for USAF component refurbishment.

## 2. Microhardness

Coating hardness is an excellent indicator of potential wear resistance in well-consolidated sprayed coatings, where weaknesses at splat boundaries would not be limiting. Microhardness was measured with a Shimadyer microhardness tester. Three adjacent locations were tested at each sample position and then averaged to provide overall hardness indications. The hardness values ranged from 400 to 1500 DPH (see Figure 14). Hardness values varied appreciably at a single position, depending on the exact nature of the microstructure. For example, values obtained near a splat boundary were often lower than within a splat, due to the lower strength of the boundary region. In addition, local microstructures varied from amorphous to dendritic, depending on characteristics such as droplet size and proximity of the impacting droplets to the base metal for prompt heat transfer.

Even after averaging, some spread was evident in microhardness values within each sample. This spread was mainly caused by dissimilar solidification rates between the thinly tapered edges and the thicker crowns. Heat transfer was more rapid from thinner regions, while coarser microstructures (larger dendrites) were generally found in the coating crowns. Unlike the porosity measurements, microhardness values tended to be grouped closely among samples from a given experiment. This reflected the fact that spraying rates, base metal speeds, and deposition temperatures were approximately the same along the length of a given specimen. The only significant exception to this trend is the group of

41
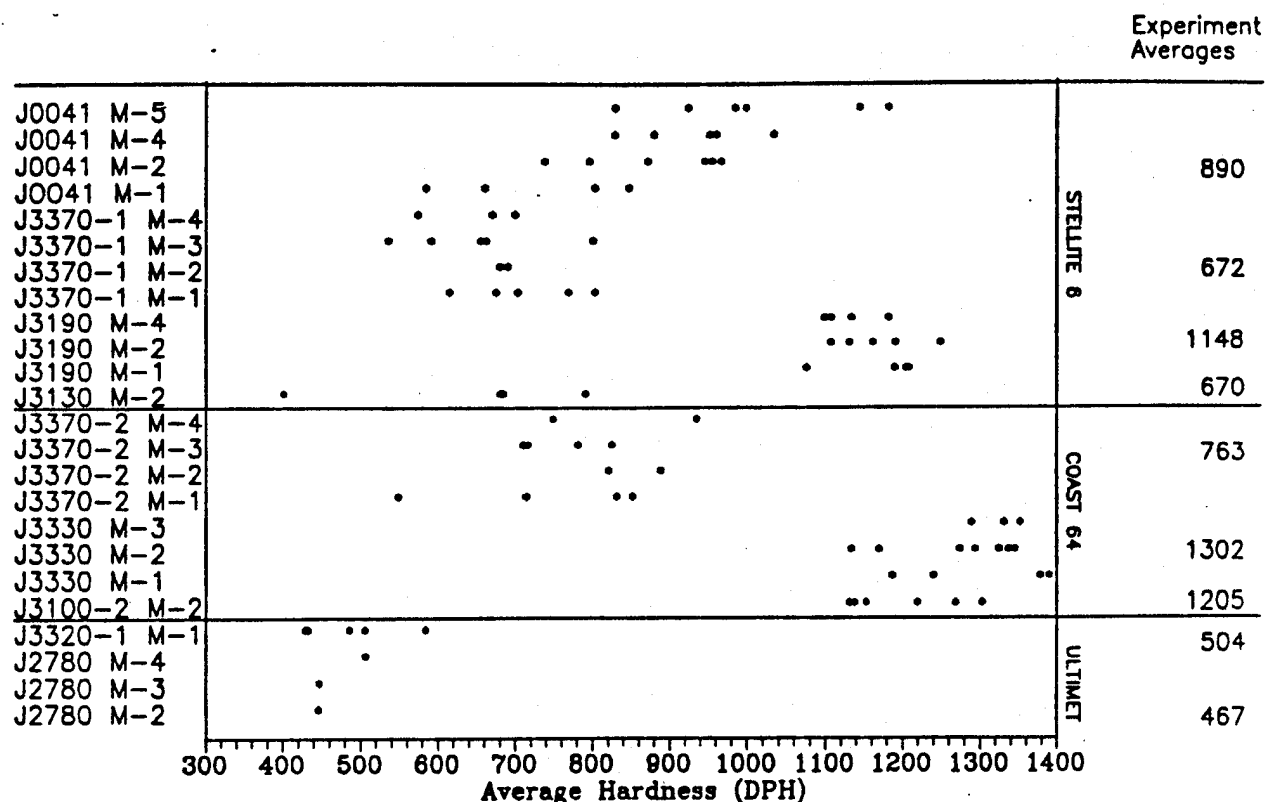
Figure 14.  Coating Hardness.

samples from the J0041 experiment, where the base metal speed was deliberately varied to induce different coating thicknesses.  Higher hardness values were associated with thinner coatings.

Grand averages of the microhardness values are shown along the right side of Figure 14 for each of the experiments.  These grand averages are most meaningful in assessing the effects of deposition conditions and alloy compositions.  Stellite 6 and Coast 64 coatings have conspicuously higher hardness values than Haynes Ultimet coatings.  This is mainly attributed to the much higher carbon contents of Stellite 6 and Coast 64 (1.1 and 0.9 weight percent, respectively, versus 0.08 weight percent in Ultimet).  The Ultimet coating contained virtually none of the hard chromium and tungsten carbides present in Stellite 6 and Coast 64, despite their otherwise similar compositions.

Figure 14 reveals significant shifts in hardness among the experiments for both Stellite 6 and Coast 64.  For Stellite 6 coatings, the

42

highest hardness values occurred for microcrystalline microstructures, which were typically created in thinner coatings at relatively cool deposition conditions. Lower values were measured on fine dendritic microstructures that experienced higher heat flux or slower heat conduction to the base metal due to a thicker coating (or a combination of the two). The lower hardness values for Coast 64 coatings were also associated with fine dendritic microstructures. However, the higher values were obtained from amorphous (or nanocrystalline) deposits, instead of microcrystalline material. In both cases, finer microstructures dictate that carbide particles are smaller and more uniformly distributed than in coarser dendritic material. Coast 64 coatings tended to be slightly harder than Stellite 6 for similar deposition conditions, which may have been due to their higher tungsten content (19 versus 4 weight percent, respectively). The tungsten may strengthen the cobalt-based matrix around the dispersed carbides, since the amount of carbide ceramic (mostly chromium carbide) would be nearly identical in the two alloys. However, because of its distinctly larger atomic mass and size, tungsten may also inhibit solidification and promote amorphous microstructures with finer carbide dispersions.

Significantly, no hardness differences related to microstructure variations are found between the Haynes Ultimet coatings. The J3320-1 experiment produced a fine dendritic microstructure very similar to those of the soft J3370-1 Stellite 6 and J3370-2 Coast 64 coatings. The J2780 Ultimet experiment involved a higher heat flux and a fully molten deposit that formed a diffusion bond with the base metal; the J2780 samples exhibited much coarser dendrites than observed elsewhere. The absence of a noticeable difference in the Ultimet hardnesses, despite the microstructural differences, may also be related to the low carbide content. Strengthening from fine carbide dispersions apparently requires a larger concentration of carbides than is found in Ultimet.

For perspective, all hardness values measured represent a major increase above the parent stock, according to the manufacturers' product literature. Haynes Ultimet has a typical hardness of 300 DPH in the

43

mill-annealed condition (no cold work), whereas the as-sprayed values are at least 50 percent harder than can be achieved with conventional casting. Minimum hardness values quoted for Stellite 6 and Coast 64 are for a weld-overlayed condition, since these alloys were used for hardfacing before modern coating technologies were developed. For standard gas tungsten arc welds, hardnesses of approximately 400 and 450 DPH can be expected for Stellite 6 and Coast 64, respectively. Such high-temperature weld overlays normally consist of dendrites so coarse that they extend completely through the coating thickness. Their carbide particles are much larger and more widely separated than in the rapidly solidified, spray formed coatings. The coatings with the highest grand averages (Figure 14) are among the hardest metals ever produced by any technique, near the hardness of cemented-carbide cutting tools that are at least 90 weight percent ceramic.

### 3. Adhesion Strength

The adhesion of spray formed coatings relies upon mechanical bonding to the base metal surface. The steel strips employed in Phase II were roughened with coarse alundum grit before spraying. For strong coating adhesion, droplets at the leading edge of the spray plume must wet the grit-blasted surface and fill in all indentations before completely solidifying. Adhesion strength was determined using a uniaxial pull-test (ASTM 633-69) conducted on an Instron Model 1128 load-test machine. The samples were trimmed so that the load would be distributed over exactly 0.049 in.$^2$ of bonded area. The crosshead drive was set at the slowest speed available--0.002 in./min--to prevent abruptly tearing a sample apart.

Results from all valid Phase II tests of mechanical bond strength are displayed in Figure 15. Ultimet values were not obtained; Samples J2780 A1 and A2 failed at the epoxy that attached the pulling fixtures, and J3320 and J3370-2 A2 failed prematurely by peeling under pull-piece misalignment. The Stellite 6 and Coast 64 samples all failed sharply and abruptly. As with the porosity measurements, the adhesion strength varied widely, and no significant correlation could be made with
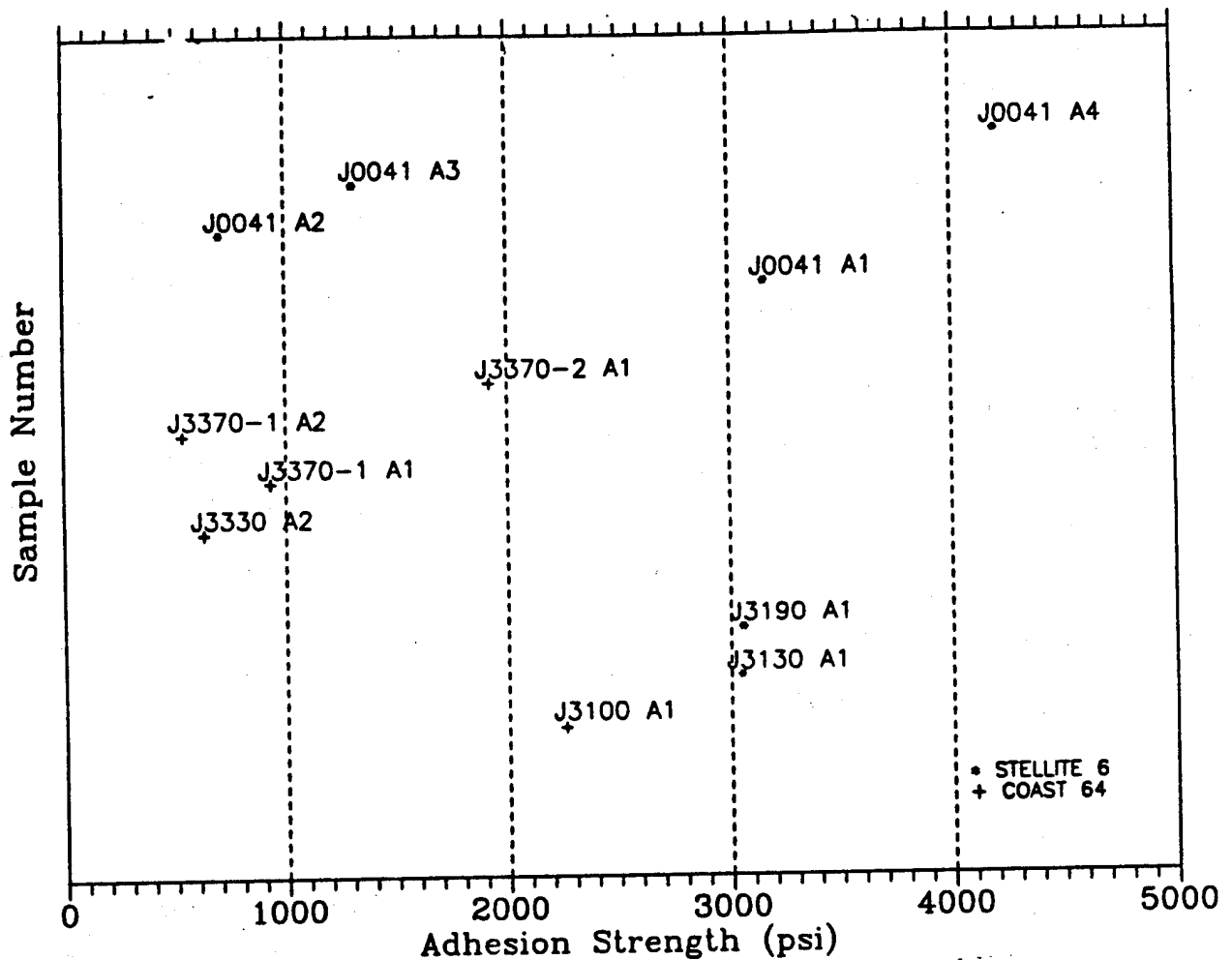
**Figure 15. Coating Adhesion Strength.**

coating parameters. The large variation in adhesion strength was most glaringly demonstrated by the four samples from the J0041 experiment, where values ranged from 700 to 4200 psi.

Several samples experienced local rupture or fracture within the coating layer instead of failing cleanly along the coating/base metal interface. This was particularly evident on Stellite 6 samples J0041 A2 and J0041 A3 and Coast 64 sample J3330 A2, where appreciable patches of coating remained attached to the base metal. Rupturing in the two J0041 samples was initiated at large pores caused by either gas entrapment or incomplete consolidation, because both phenomena occurred to varying extents in the J0041 coating. Metallography revealed that the J3330 coating delaminated under the central crown during cooldown, presumably from base metal warping under differential thermal stress. This coating

45

fractured along the thin, brittle edges of the deposit, leaving those portions attached to the base metal.

Stellite 6 samples J3370-1 A1 and A2 failed cleanly along their interfaces, but the base metal surfaces showed round discolored areas as large as one millimeter in diameter. Metallography suggested that these large interfacial pores were created by gas entrapment; the Stellite 6 had dribbled along the nozzle roof before impacting the base metal in irregular forms, rather than as fine droplets. Consequently, the relatively low adhesion strengths here may indicate poor nebulization from unequal aspiration.

Bond strength on the remaining six samples ranged from 1900 to 4200 psi, which was slightly better than Phase I values and in the realm of plasma-sprayed nonferrous coatings (Reference 4). Consistently producing greater bond strength will require reducing interfacial porosity by improving nebulizer stability, as well as minimizing delamination due to differential thermal stress. Base metal preparation also must be investigated further, including the effects of cleaning, roughening, and preheating.

# SECTION IV
## VIABILITY OF SPRAY COATING TECHNOLOGY

Applying the Phase II results to the needs of the Air Logistics Centers necessarily involves considerable speculation. Yet, many findings can be assessed with regard to these requirements and areas requiring additional development can be identified.

## A. HIGH TEMPERATURE OPERATION

One of the main objectives of Phase II was to investigate the practicality of extending the low temperature spray coating technology of Phase I to a realistic temperature range for spraying metals that could replace electroplated chromium on worn USAF components. Phase II clearly demonstrated that components can be heated sufficiently to enable spraying high performance hardfacing alloys with the potential for surpassing the properties of electroplated chromium coatings. No fundamental reasons emerged during Phase II that would prevent spray coating from being adopted for USAF components. Nevertheless, elevating certain component temperatures was only achieved with difficulty, and spraying pure chromium was not found to be practicable with the current spray system.

The spray chamber and inert gas purging approach restricted oxidation to a negligible extent, even for melt temperatures approaching 2000°C. Melting and pouring of metal feedstock also appeared viable to this temperature without accelerated deterioration of standard refractory crucibles, assuming that trace concentrations of oxygen can be tolerated within the coatings. A vacuum chamber to degas components before spraying was not necessary.

Resistance heating of the incoming nebulizing gas was not suitable for stable, predictable operation at temperatures above 600°C. In Phase II, the inability to preheat the argon nebulizing gas to above the melting point of the metal being sprayed necessitated large amounts of melt

47

superheat that increased erosion of the base of the nozzle tundish. Induction heating using refractory metal elements should permit greater gas temperature flexibility and reduce required melt temperatures.

As discussed earlier, degradation of the boron nitride nozzles at elevated temperatures was confined to erosion at the tundish base and to a reaction between the graphite susceptor and the nozzle exterior. Melt erosion limited nozzle lifetime to a small number of spray coating experiments, while the graphite-boron nitride reaction ultimately prevented spraying pure chromium. However, both problems can be solved by using different materials--boron nitride was selected primarily for ease of fabrication while the nozzle geometry was being optimized. Significantly, even the highest melt temperatures did not detectably affect the alumina tubes used as liquid orifices. Replacing graphite with a refractory metal susceptor would allow additional refinements of boron nitride nozzle geometries, and a wide choice of materials is available for fabricating nozzles once the dimensions have been firmly established.

## B. NEBULIZER BEHAVIOR

The nebulizer design was adequate for spraying high melting point hardfacing alloys with very promising properties. Nevertheless, several interrelated problems with initiating and maintaining equal aspiration through all of the liquid orifices were identified. Unequal aspiration was manifested in a wider than desired droplet size distribution, uneven deposit thicknesses, entrapped gas pores, and less than uniform microstructures.

The most direct method for improving near-term nebulizer behavior would be to adopt a single-orifice nozzle of circular cross section. Aspiration would be more stable and predictable, and shearing into fine droplets would be virtually guaranteed in a smaller area throat. Such a nozzle would be well-suited for repairing narrow wear grooves in bearing races, such as supplied by Tinker Air Force Base. The Gaussian thickness profile from a

48

circular nozzle would closely match the depth contour observed in these grooves, and masking could be employed to remove deposit edges.

Nozzles of rectangular geometry still appear viable for large-area applications, though further development is required. Appreciably wider nozzles with substantially more orifices would be less susceptible to edge effects, such as reduced suction near the sides of the tundish base, that produced noticeably crowned deposits in Phase II. Another approach would be to reduce the sensitivity of aspiration to liquid orifice suction everywhere at the tundish base by, for example, a pressurized melt feed or a deeper melt head. The progress that is expected in Phase III in two-dimensional nozzle modeling will likely lead to other possible long-term refinements.

## C. COATING PROPERTIES

Perhaps the most encouraging Phase II finding was the dramatic increase in coating hardness that was achieved by rapid solidification. Producing uniformly fine dispersions of chromium carbides in Stellite 6 and Coast 64 created coatings approximately three times harder than weld- overlayed parent material with coarse dendrites. Not only would the fine carbides resist pullout during in-service wear, but they would also reinforce the metal matrix by dispersion strengthening. Furthermore, coatings with hardness in the 1100 to 1300 DPH range would be harder than electroplated chromium, and would approach the hardness of cemented carbide cutting tools. The substantial chromium contents of these cobalt-based alloys would ensure comparable corrosion resistance to electroplated chromium. A major improvement in component service life could thus be anticipated, wherever service temperatures were low enough to prevent significant coarsening of the microstructure by equiaxed grain growth. Phase II efforts confirmed that these high performance coatings can be ground mirror-smooth to meet tight dimensional tolerances.

Average coating porosity of two area percent, surpassing that of conventional thermal sprayed coatings, is promising for eventual

49

application at Air Logistics Centers. The pores were never connected, so corrosion protection would not be jeopardized. In addition, porosity could probably be reduced by nebulizer optimization that yielded a uniform plume of finer droplets for better consolidation without entrapped gas.

Adhesion tests were complicated by several effects, making it difficult to predict the strengths that can be expected on production coatings. Valid measurements ranged widely, from 500 to 4200 psi; the higher values were in the accepted range for conventional thermal sprayed coatings. Improved nebulizer behavior would almost certainly raise these values, because uniformly fine droplets would reduce porosity from both incomplete splat consolidation and gas entrapment. Less porosity at the base metal surface would directly increase mechanical bonding, while less bulk porosity would eliminate rupturing within the coating layers. Differential thermal stress also had a major influence on adhesion, particularly for thicker coatings. Large stresses can induce delamination along the interface and fracturing in brittle coatings; both phenomena were observed in Phase II samples. These effects are not unique to spray coating and occur in hardfacing techniques from weld-overlaying to plasma spraying (Reference 5). Uniform preheating of the base metal so that the coating and base metal shrink to similar extents, leaving only a small compressive stress in the coating to resist fatigue cracks, is the preferred solution. Preheating and the effects of cleaning and roughening techniques on adhesion strength were not systematically investigated in Phase II.

The microcrystalline and amorphous coatings of Stellite 6 and Coast 64 often exhibited brittle fractures at positions of stress concentration. These alloys are normally brittle, but rapid solidification may have exaggerated this tendency. Alloy composition adjustments may be able to reduce fatigue cracking while maximizing high hardnesses and other benefits of spray formed coatings. For example, rapidly solidified nickel-chromium and iron-chromium alloys may be less brittle than cobalt-chromium alloys, and they would be less expensive.

50

# SECTION V
## MODELING

The ability to understand and predict a) the flow properties of a gas carrying particles or droplets and b) the deposition, subsequent heat transfer from, and solidification of those particles is important in the design, development, and optimization of spray coating systems. The objective of Task 1 was to review existing models and evaluate their potential for numerically simulating spray deposition. The objective of Task 3 was to begin numerical simulations of two-phase nozzle dynamics, incorporating Phase I data on liquid breakup and plume geometry and Task 2 results on nozzle characterization with high temperature gas flow and metal droplets in the gas stream.

## A. TASK 1: MODELING PARTICLE CONSOLIDATION

Solidification of the sprayed particles is a very complex process. A simplified approach was deemed a necessary first step in modeling heat transfer and solidification, so a one-dimensional model of the deposition, heat transfer, and solidification process was constructed. It was assumed that the parent metal to be sprayed was a sheet or flat plate and that the layers of coating material were flat and parallel to the parent metal surface. At the time it was deposited, the coating material was assumed to have sufficient liquid content to permit this flat layer; it was also assumed that the material was deposited rapidly enough that a homogeneous deposit existed (as opposed to droplet splats that solidify so rapidly that a local flake structure occurs). Solidification was assumed to be appropriately represented as an equilibrium process.

The computer model solved the transient heat conduction equations using a simple forward Euler finite difference method. The model structure consisted of a parent layer (onto which a spray was deposited) and an arbitrary number of thinner layers that could be added sequentially to the parent layer to simulate a growing spray deposit. The layers were

sequentially added over the same time frame in which the actual sprayed layer was deposited. The parent layer and each sequentially added spray layer were discretized with a specified number of mesh points. The number of mesh points assigned to each layer was problem dependent, but 25 mesh points for the parent layer and five mesh points for each of five sequentially added layers were typical.

The computer program permitted convective boundary conditions to be applied to the parent material on the surface opposite the sprayed coating and convective and radiative boundary conditions to be applied at the surface of the sprayed layer onto which new droplets were falling. The program also allowed convective heat flow resistance to be applied at the interface between the parent material and the sprayed layers to simulate an imperfect thermal contact between the two surfaces. Equilibrium phase change was accounted for with solidification occurring over a specified temperature range. The program automatically selected a stable time step and outputs temperature and solid fraction for each spatial mesh point at user specified times in the transient process.

The results of the model are best illustrated with a typical example. Consider the problem of identifying the temperature and solidification histories of the parent material and the sprayed coating for a steel plate 1 cm thick with a 1 mm thick layer of Stellite 6. Assume that the layer is sprayed uniformly (in time) over a 0.5 s interval. Other relevant parameters assumed for this particular analysis include:

- Convective gas temperature, back side of parent layer = 300 K
- Convective gas temperature, spray layer top surface = 900 K
- Radiative boundary temperature, spray layer top surface = 900 K
- Initial temperature of steel parent layer = 300 K
- Temperature of sprayed material entering deposit = 1630 K
- Convective coefficient, back side of parent layer = 0.000 $W/K \cdot cm^2$
- Convective coefficient spray, layer top surface = 0.057 $W/K \cdot cm^2$
- Convective resistance coefficient at interface = 0.075 $W/K \cdot cm^2$
- Sprayed layer emissivity = 0.28
- Stellite 6 mass density = 8.387 $g/cm^3$
- Stellite 6 liquidus temperature = 1630 K
- Stellite 6 solidus temperature = 1533 K
- Stellite 6 liquid specific heat = 0.70 $J/g \cdot K$
- Stellite 6 solid specific heat = 0.423 $J/g \cdot K$

- Stellite 6 heat of fusion = 315 J/g

The model was run for 8.0 s (physical time) from the commencement of spraying. The sprayed layer was predicted to be totally solidified in just slightly under 1.5 s (see Figure 16), and after 8.0 s the temperature difference between the sprayed layer and the base metal was about 260 K (Figure 17). Over much of the time, the temperature distribution in the layers was fairly uniform, but the temperature gradients were more significant early in the process. The solid fraction distribution during solidification was not uniform through the thickness, as expected.

This simple one-dimensional model gave valuable insight into the thermal/solidification response of coatings that fall within the stated assumptions; in general, these assumptions will be met for thick coatings that are deposited rapidly. For thin coatings, especially those with relatively slower deposition times, significant solidification can occur in the droplet splat so the assumption of equilibrium states and one-dimensional heat transfer would not be valid. For the coatings for which these assumptions do not hold, significantly more work needs to be done to incorporate their more complex governing features. It appears that coupling a two-phase mixture theoretical approach with a rezoning Lagrangian dynamics approach to represent the droplet splat dynamics would be a feasible way to pursue this problem. Another approach with strong merit is the quasi-particle method in which the droplet splat dynamics is represented as a collection of quasi-particles with a Leonard-Jones type stress representation, in a pseudo-molecular dynamic fashion. Between these two approaches lie some hybrid methods that may also prove feasible. While these methods have never been applied to this type of problem, it is believed that this problem is tractable, and its solution is necessary to ultimately produce "coatings by design".

## B. TASK 3: MODELING NOZZLE DYNAMICS

A primary difficulty in modeling gas-particle (droplet) flow arises from the fact that the flow of the gas (continuum) phase is most
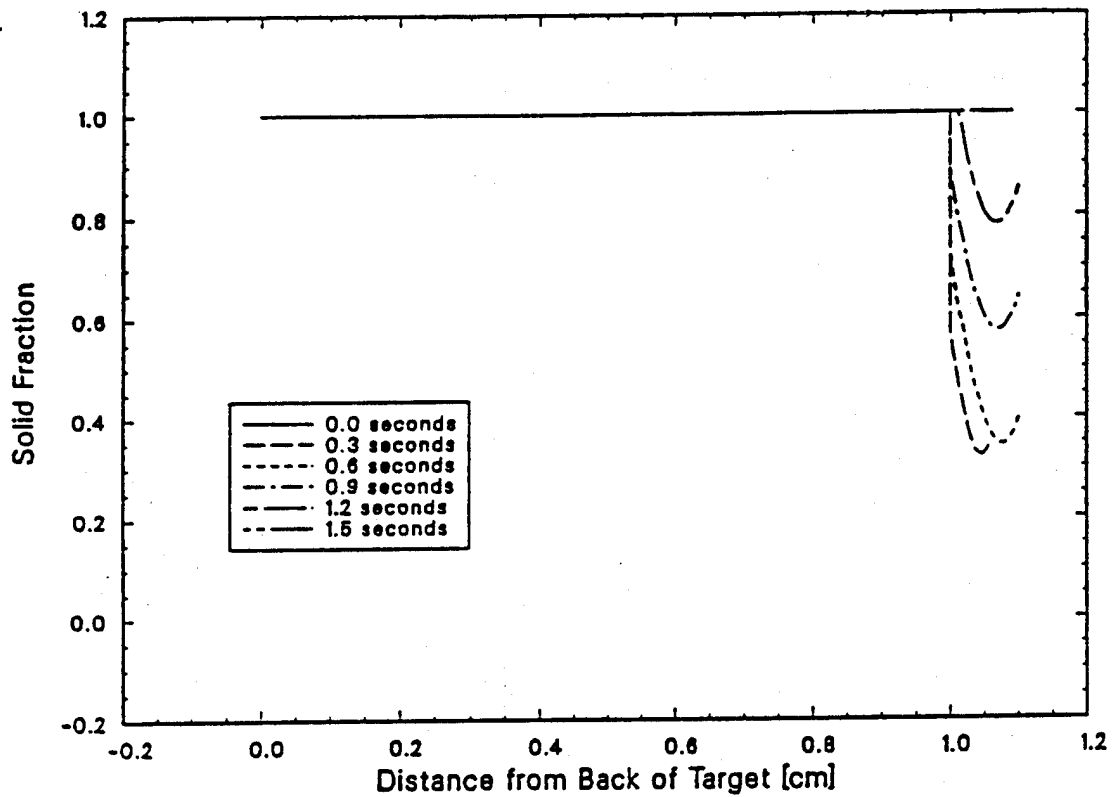
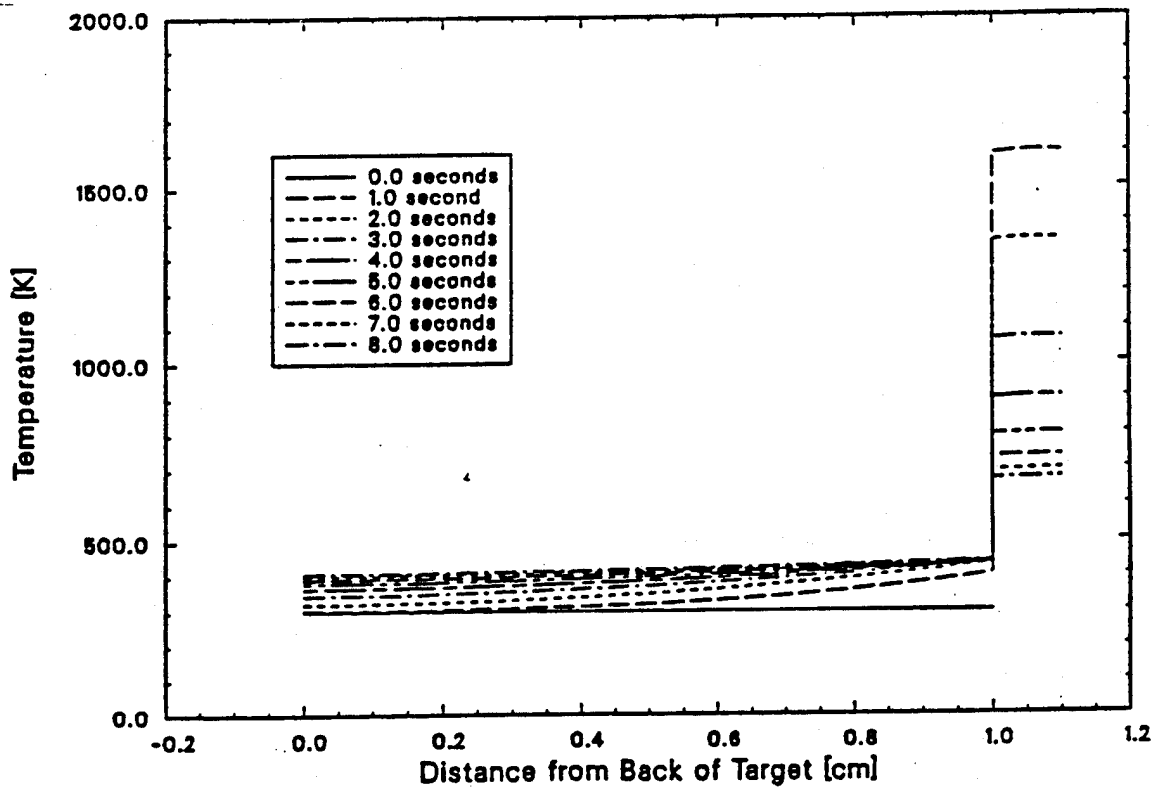Figure 16.   Solid Fraction during Coating Deposition.



Figure 17.   Temperature during Coating Deposition.

conveniently described by an Eulerian system, whereas the particle (discrete) phase is more appropriately handled from a Lagrangian viewpoint. Another feature of two-phase flow that complicates modeling is coupling between phases, i.e., the particles and gas exchange mass, momentum, and energy. For example, for slowly moving particles in an accelerating gas flow, the aerodynamic drag force will cause a momentum transfer from the gas to the particles. The resulting decrease in momentum of the gas changes the gas flow field which, in turn, affects the particle trajectories. If the particles are hotter than the local gas, then an energy (heat) transfer will occur. The particle may cool (or a molten droplet begin to solidify), while the gas gets hotter. The increased gas temperature may affect the gas dynamics which, in turn, will affect the particles dynamics (trajectory). The overall complexity of the coupling phenomena, which are due to nonequilibrium between the gas and particles (droplets), is apparent when mass, momentum, and energy are all considered.

Another type of nonequilibrium occurs with small droplets of molten material that undergo in-flight cooling. Because the droplets are small, there are significantly fewer nucleation sites from which solidification can commence. Fewer nucleation sites together with rapid cooling can lead to significant undercooling (i.e., reaching temperatures below the normal solidification temperature) before the onset of solidification. When solidification does commence, the rapid evolution of latent heat (due to conversion from liquid to solid) and the droplet's limited ability to transfer this thermal energy to the gas can produce rapid droplet (particle) temperature increases until the latent heat evolution balances the convective heat removed to the gas. This phenomenon is known as *recalescence*.

The basic methods and models developed under a related Department of Energy (DOE) program were modified and applied to this project. A nonequilibrium, quasi one-dimensional model was used to simulate the entire nozzle and plume regions with full aerodynamic and energetic coupling between the droplets (particles) and the transport gas and with coupled liquid injection/aspiration (mass loading) into the gas stream. This model

is executed with two computer programs run in succession, one for the nozzle region (nozzle inlet plane to nozzle exit plane) and one for the plume region (nozzle exit plane to sprayed surface). These programs are very easy and economical to run and give the experimenter a good indication of the effect of varying system parameters, identifying some easily overlooked, nonlinear effects. These programs allow the user to develop a "feel" for the system response. The one-dimensional models may also be valuable for the construction of algorithms for the control of spray coating processes. Lastly, these one-dimensional models give direction to the two- and three-dimensional simulations and serve as a test bed for particle dynamics and energetics submodels. For purposes of optimizing the spray nozzle design, however, the one-dimensional models were not adequate. During the later part of this task emphasis was shifted to a two-dimensional simulation. A grid generation code was used to generate a two-dimensional grid of the spray nozzle for use with a two-dimensional gas dynamic simulation.

Viscous, turbulent gas dynamic simulations were carried out in two-dimensions but without particles/droplets. We have the basic capability to include the fully coupled particle (droplet) field with the gas dynamics in two- and three-dimensions as a result of ongoing development activity for DOE; however, at the conclusion of this task we were at the point of analyzing and balancing the gas field separately, a necessary step prior to the addition of an injected droplet field.

1. Quasi One-Dimensional Nozzle and Plume Modeling Methodology

Spray coating technology involves transonic gas-particle (droplet) flow through a de Laval nozzle and subsonic free jet flow from the nozzle to the sprayed surface. To a first order approximation, this complex phenomenon can be treated in a quasi one-dimensional manner. The model treats the steady gas field through a conservative variable approach and treats the coupling phenomena between the gas and particles (droplets) through source terms as described by Berry (Reference 6). As in Reference 6, the basic conservation principles are directly applied to a

control volume or computational cell. The procedure is to solve the flow through one control volume after another until the entire flow field solution is obtained.

### a. Flow Conservation Equations

Consider the quasi one-dimensional flow of a particle-laden gas in a duct of uniformly varying cross-sectional area as shown in Figure 18. For this control volume the mass conservation principle for steady gas flow is

$$\rho_2 u_2 A_2 = \rho_1 u_1 A_1 \tag{1}$$

where $\rho$ is the gas density, u is the gas velocity, A is the cross-sectional area, and the subscripts indicate the location. This equation assumes that particles (droplets) occupy negligible volume in the gas field, which is a good approximation for spray coating nozzles.
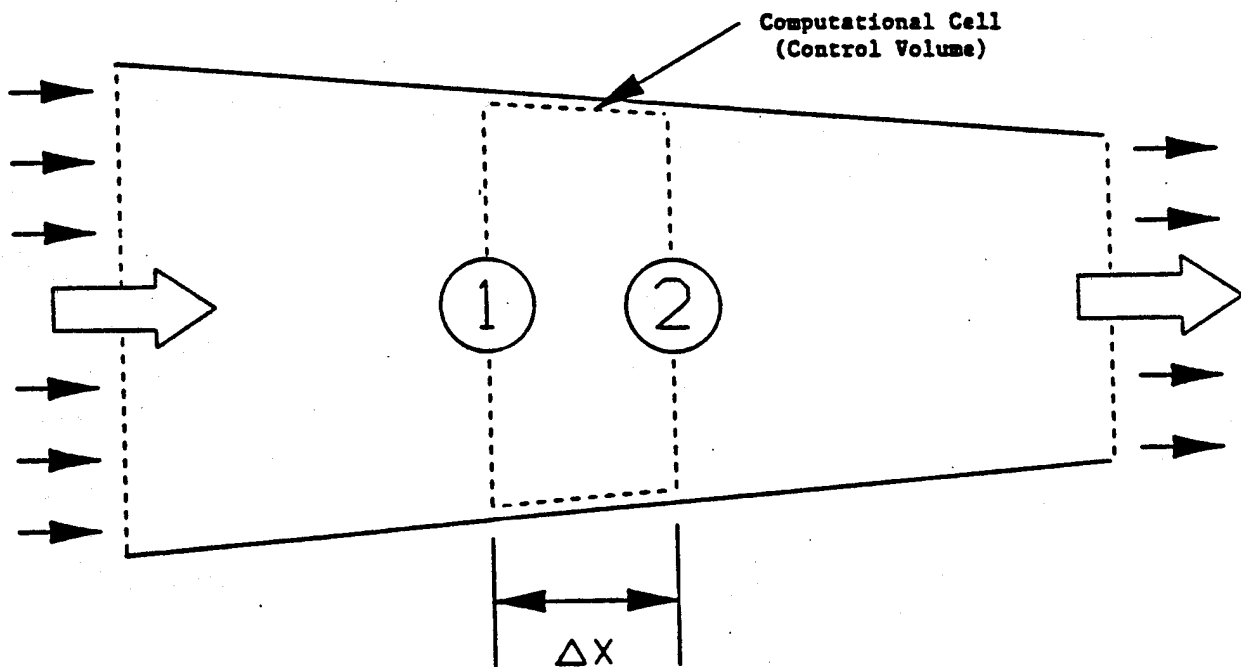


Figure 18. Computational Cell for Numerical Model.

Applying the momentum principle for the control volume in terms of the flow properties gives

$$p_2 A_2 + \rho_2 u_2^2 A_2 = p_1 A_1 + \rho_1 u_1^2 A_1 + \frac{(p_1 + p_2)(A_2 - A_1)}{2} + \Delta \dot{M}_p - F_{wx} \tag{2}$$

where p is the gas pressure at locations 1 and 2, $\Delta \dot{M}_p$ is the "source" term for momentum due to the presence of the particles (evaluated from the equations of motion for the particles in the flow field), and $F_{wx}$ is the shear force at the wall opposing fluid motion.

The energy conservation principle for the control volume is

$$\rho_2 u_2 A_2 \left[ h_2 + \frac{1}{2} u_2^2 \right] = \rho_2 u_1 A_1 \left[ h_1 + \frac{1}{2} u_1^2 \right] + \Delta \dot{E}_p + \dot{Q} \tag{3}$$

where h is the enthalpy of the gas at location 1 and 2, $\Delta \dot{E}_p$ is the "source" energy due to the presence of the particulate phase, and $\dot{Q}$ is the thermal energy added to the flow per unit time between locations 1 and 2 (heat transfer from the walls).

In a one-dimensional flow without source terms (gas only), wall friction, or heat transfer, the combination of variables $\rho u A$, $pA + \rho u^2 A$

and $\rho u A \left[ h + \frac{u^2}{2} \right]$ are conserved, even across shock waves. In flow fields with particle effects, wall friction, and heat transfer, these variables can still reasonably be expected to change more slowly than the primitive variable. Therefore, from a mathematical standpoint, these variables make better dependent variables and will be introduced

$$X = \rho u A \tag{4}$$

$$Y = pA + \rho u^2 A = pA + Xu \tag{5}$$

$$Z = \left[ h + \frac{u^2}{2} \right] \rho u A \tag{6}$$

as the *conservative variables*. The primitive variables can be recovered from the conservative variables as follows. The enthalpy can be expressed (assuming a calorically perfect gas) as

$$h = c_g T_g = \left[ \frac{\gamma}{\gamma - 1} \right] \left( \frac{p}{\rho} \right) \tag{7}$$

where $c_g$ and $T_g$ are the specific heat and temperature of the gas, respectively, and $\gamma$ is the specific heat ratio for the gas. Substituting equations (4), (5), and (7) into equation (6) yields

$$Z = \left[ \frac{\gamma}{\gamma - 1} \right] Yu - \left[ \frac{\gamma + 1}{\gamma - 1} \right] X u^2 \tag{8}$$

and solving for u gives

$$u = \left[ \frac{\gamma}{\gamma + 1} \right] \frac{Y}{X} \left\{ 1 \pm \left[ 1 + 2 \left[ \frac{1 - \gamma^2}{\gamma^2} \right] \frac{XZ}{Y^2} \right]^{1/2} \right\} \tag{9}$$

The negative sign on the radical in equation (9) applies to *subsonic* flow and the positive sign to *supersonic* flow. The flow is *sonic* when the discriminant is zero. With the gas velocity determined by equation (9), the gas density is obtained from equation (4) and the pressure from equation (5).

In terms of the dependent variables X, Y, and Z the governing equations (1) through (3) are written .

$$X_2 = X_1 \tag{10}$$

$$Y_2 = Y_1 + \Delta \dot{M}_p + \left[ \frac{p_1 + p_2}{2} \right] \left( A_2 - A_1 \right) - F_{wx} \tag{11}$$

$$Z_2 = Z_1 + \Delta \dot{E}_p + \dot{Q} \tag{12}$$

b.  Particle Source Terms

The source terms for the effects of particles on the gaseous phase are evaluated by determining the particles' motion and temperature history.  The momentum and energy source terms are obtained by integrating the equations of particle motion and heat transfer using the velocity, pressure, and temperature fields of the gas.  The Lagrangian approach is used for this integration.  The momentum source term due to a particle in the control volume is

$$\Delta \dot{M}_p = \dot{m}_p \left( v_1 - v_2 \right) \tag{13}$$

where $\dot{m}_p$ is the mass flow rate of particles (spray liquid mass flow rate) and v is the velocities of the particles at locations 1 and 2.  The difference in particle momentum between locations 1 and 2 augments the gas-phase momentum.  The particle velocity change is approximated by integrating the equation of motion of a spherical particle.

$$m_p \frac{dv}{dt} = C_d \rho \left( u - v \right) |u - v| \frac{A_p}{2} + m_p g \tag{14}$$

where $m_p$ is the mass of a particle, $A_p$ is its projected area, $C_d$ is its drag coefficient, and g is the acceleration due to gravity.  In this equation aerodynamic forces due to pressure gradients, virtual mass

effects, and Basset forces are neglected, as are particle-particle collisions, particle-wall interactions, and turbulent dispersion of particles. The body force term is excluded for horizontal flows. This equation can be rewritten (neglecting the gravity term) as

$$\frac{dv}{dt} = \frac{\lambda}{\tau_a}(u-v) \tag{15}$$

where

$$\lambda = \frac{Re}{24} C_d$$

$$\tau_a = \frac{\rho_p D_p^2}{18\mu}$$

$$Re_p = \frac{\rho|u-v|D_p}{\mu}$$

where $D_p$ is the particle diameter, $\rho_p$ is the particle mass density, $\mu$ is the gas viscosity, and $Re_p$ is the Reynolds number based on particle diameter. The factor $\tau_a$ is the *aerodynamic response time*, roughly the time it takes a particle released from rest to achieve 63% of free stream velocity (in Stokes flow where $\lambda=1$, $C_d=24/Re_p$). The drag coefficient, $C_d$, used for $Re_p < 300,000$ is (Reference 7)

$$C_d = \frac{24}{Re_p}\left(1 + 0.15 Re_p^{0.687}\right) + \frac{0.42}{1 + 4.25 \times 10^4 Re_p^{-1.16}} \tag{16}$$

This equation may be integrated between location 1 and 2 to get

$$v_2 = \left[\left[\frac{\lambda \Delta x}{\tau_a}\right]^2 + v_1^2 + 2\left[\frac{\lambda \Delta x}{\tau_a}\right]u\right]^{1/2} - \left[\frac{\lambda \Delta x}{\tau_a}\right] \tag{17}$$

where $\Delta x$ is the distance interval between locations 1 and 2.

The energy equation for a solidifying droplet in a gas stream can be reasonably approximated with the same temperature for each phase (solid and liquid), so

$$m_p (c_p)_m \frac{dT_p}{dt} = \pi D_p k \, Nu \, (T_g - T_p) - 4 \pi r_i^2 \dot{r}_i \rho_1 H \tag{18}$$

where $(c_p)_m = (c_p)_s f_s + (c_p)_1 (1-f_s)$ is the specific heat of the droplet taken as a solid fraction $(f_s)$ weighting of the solid and liquid specific heats, $k$ is the gas thermal conductivity, $T$ is the temperature of the respective gas and droplet, $H$ is the heat of fusion for the droplet, and $Nu = hD_p/k$ is the Nusselt number (where $h$ is the convective heat transfer coefficient). Equation (18) is based on a spherical droplet with a spherical interface of radius $r_i$ separating the inner liquid region from the outer solid region. The velocity with which the interface advances through the droplet, $\dot{r}_i$, is given by (Reference 8)

$$\dot{r}_i = -A (T_m - T_p)^n$$

where $T_m$ is the equilibrium melt temperature and $A$ and $n$ are empirical coefficients. Equation (18) can be written as

$$\frac{dT_p}{dt} = \frac{Nu}{2} \frac{T_g - T_p}{\tau_t} - \frac{6 \dot{r}_i D_i^2 H}{(C_p)_m D_p^3} \tag{20}$$

where

$$\tau_t = \frac{\rho_p (c_p)_m D_p^2}{12 \, k}$$

is the *thermal response time*, roughly the time it takes a particle to achieve 63% of free stream temperature (in Stokes flow where Nu=2 and where

no phase change occurs). The Nusselt number quantifies the heat transfer to and from the particle and depends on the particle Reynolds number and gas Prandtl number. For the spherical particles assumed here, the relationship used is (Reference 9)

$$Nu = 2 + 0.6 Re_p^{0.5} Pr^{0.333} \tag{21}$$

Equation (20) can be integrated between locations 1 and 2 in a semi-implicit manner to yield

$$T_{p2} = \frac{T_{p1} + \dfrac{N \Delta x\, T_{g2}}{(v_1 + v_2)\, \tau_t} - \dfrac{12\, D_i^2\, H \Delta x\, \dot{r}_i}{(v_1 + v_2)\,(c_p)_m\, D_p^3}}{1 + \dfrac{Nu\, \Delta x}{(v_1 + v_2)\, \tau_t}} \tag{22}$$

The energy source term due to the particles is then given by

$$\Delta E_p = \dot{m}_p \left[ \frac{v_1^2 - v_2^2}{2} \right] + \Delta E_{th} + \dot{m}_p\, \frac{(D_i)_1^3 - (D_i)_2^3}{D_p^3}\, H \tag{23}$$

where

$$\Delta E_{th} = \dot{m}_p \{ [f_{s1}(c_p)_s + (1 - f_{s1})(c_p)_l]\, T_{p1} - [f_{s2}(c_p)_s + (1 - f_{s2})(c_p)_l]\, T_{p2} \} \tag{24}$$

which represents the difference in particle energy in traveling between locations 1 and 2 and a resulting source of energy in the gas phase.

### c. Liquid Injection

The liquid metal feed model assumes a simple orifice-type flow relation for the tube connecting the tundish with the nozzle, which couples the liquid feed rate with the local nozzle gas pressure. The mass flow

rate of liquid injected into the nozzle (which becomes $\dot{m}_p$ in the nozzle) is

$$\dot{m}_1 = C_{dis} \, \rho_1 \, A_{dis} \sqrt{\frac{2 \, (p_{surf} - p_{nozz})}{\rho_1} + 2 \, g \, h_{surf}} \qquad (25)$$

where $C_{dis}$ is the discharge coefficient, $\rho_1$ is the liquid mass density, $A_{dis}$ is the flow area of the tubes connecting the tundish with the nozzle, $p_{surf}$ is the (gas) pressure at the top liquid surface in the tundish, $p_{nozz}$ is the nozzle gas pressure at the local point of injection, and $h_{surf}$ is the height from the nozzle injection location to the top liquid surface in the tundish (assumed to be maintained constant).

### d. Computational Scheme

The computational scheme solves the flow field in a step-wise sequential manner. Knowing the flow properties $p_1$, $T_{g1}$, $T_{p1}$, $u_1$, and $v_1$ at location 1, the flow properties $p_2$, $u_2$, and $T_{g2}$ at location 2 are obtained by using equations (9) through (12) for the gaseous phase and equations (17) and (22) for the particulate phase. Since these nonlinear equations are coupled, when the dependent variables are computed at location 2 (given values at location 1) and primitive variables are needed from location 2, approximations are made for these primitive variables (initially, the same as at location 1); they are subsequently updated from location 2 dependent variables in an iterative fashion (Reference 6). The iteration continues until location 2 variables fail to change within a predetermined value. With the computation of one cell complete, the scheme proceeds to the adjacent downstream cell where the procedure is repeated. If convergence cannot be achieved within a relatively few number of iterations, the scheme reduces the cell size automatically and begins the process again for the new, smaller cells. This typically occurs when changes occur very rapidly over a very short distance, such as during recalescence or at the injection location. The overall philosophy of the algorithm is to adjust the inlet gas velocity until proper choking

conditions have been met at some location within the nozzle (usually in the vicinity of the throat), whereupon the shock location is adjusted until correct nozzle outlet pressure is attained to within a predetermined value. In the computer program this process is "transparent" to the user and seems to be quite robust.

### e.  Plume Region

After leaving the nozzle, the gas-particle (droplet) flow becomes a free jet or plume, until it reaches the base metal being sprayed. Some of the gas, ambient to the jet, will be entrained by the constant pressure jet and will interact with the particles, again in a coupled manner.  The plume model is similar in many respects to the nozzle model. The gas is treated in an Eulerian fashion and the particles are handled in a Lagrangian fashion.  The particle drag and heat transfer correlations are identical, as is the marching-type solution strategy.

The quasi one-dimensional, two-phase jet is assumed to expand at a constant rate; specifically, the effective (hydraulic) diameter increases linearly with distance from the nozzle exit plane

$$D_x = (1 + kx) D_{exit} \tag{26}$$

where k is an empirical constant.  The mass conservation equation with no mass coupling is

$$\dot{m}_2 = \dot{m}_1 + \Delta \dot{m} \tag{27}$$

where $\Delta \dot{m}$ is the gas mass introduced by entrainment.  The pressure field for a free jet is uniform, so there is no force due to a pressure gradient. Thus the momentum equation is

$$\dot{m}_2 u_2 = \dot{m}_1 u_1 + \dot{m}_p \left( v_1 - v_2 \right) \tag{28}$$

There is no momentum associated with the entrained fluid, because it is assumed that the fluid enters with a velocity normal to the jet direction. The velocity at location 2 is given by

$$u_2 = \frac{\dot{m}_1 u_1 + \dot{m}_p (v_1 - v_2)}{\dot{m}_1 + \Delta \dot{m}}$$ 

(29)

Considering only thermal energies, the energy equation is

$$T_{g2} = \frac{\dot{m}_1 (c_p)_{g1} T_{g1} + \Delta \dot{m} (c_p)_{g0} T_{g0} + \delta Q}{(\dot{m}_1 + \Delta \dot{m}) (c_p)_2}$$ 

(30)

where

$$\delta Q = \dot{m}_p \{ [f_{s1}(c_p)_{s1} + (1 - f_{s1})(c_p)_{l1}] T_{p1} - [f_{s2}(c_p)_{s2} + (1 - f_{s2})(c_p)_{l2}] T_{p2} + \Delta q_1 \}$$

and

$$(c_p)_2 = \frac{\dot{m}_1 (c_p)_{g1} + \Delta \dot{m} (c_p)_{g0}}{\dot{m}_2}$$

where $\Delta q_1$ is the latent heat exchanged and $(c_p)_{g0}$ and $T_{g0}$ are the specific heat and temperature of the ambient gas entrained by the plume respectively. The equation of state is

$$\rho_2 = \frac{p}{R T_{g2}}$$ 

(31)

The iteration to obtain the properties at the end of the computational step proceeds as follows. First, the density at location 2 is assumed to be the same as at location 1. Combining the momentum and mass conservation equations gives,

$$\dot{m}_2 = \sqrt{\rho_2 A_2 (\dot{m}_1 u_1 + \Delta \dot{M}_p)}$$ 

(32)

66

where $\Delta \dot{M}_p$ is again the momentum exchange with the particles. The mass entrained is

$$\Delta \dot{m} = \dot{m}_2 - \dot{m}_1 \tag{33}$$

which is then substituted into the energy equation to obtain $T_{g2}$. A new density is then solved for based on this new temperature and the equation of state. This new density is then introduced into the equation for $\dot{m}_2$ and the iteration is continued until the density at location 2 converges. The scheme then marches to the next downstream cell and repeats the process until the base metal (end of flight) is reached. The interactions with the solidifying particles are handled as they were for the nozzle calculations.

### f. One-Dimensional Model Example: Description and Results

It is desirable for the particles to be at least partly liquid when they impact the target, though the optimal liquid/solid composition remains unknown. For energy conservation, and perhaps also to enhance the properties of the coating, the liquid droplets should not be much hotter than the melting temperature at impact. Thus, it is desirable to know how variations in the process parameters affect the particle solid fraction (ratio of volume of solid to total particle volume) and the particle temperature at impact. Parametric studies were done with the quasi one-dimensional model to estimate the importance of various parameters in the spraying process.

A schematic of the spray nozzle and plume for the quasi one-dimensional model is shown in Figure 19. In this example, the material sprayed is Stellite 6, which melts/solidifies over the range of 1593 to 1624 K. The nozzle body is assumed to be maintained at 1923 K. The molten material to be sprayed enters the gas stream at the rear of the throat with a temperature of 1973 K. The environment gas is at 300 K. The parameters for this nominal case are as follows:
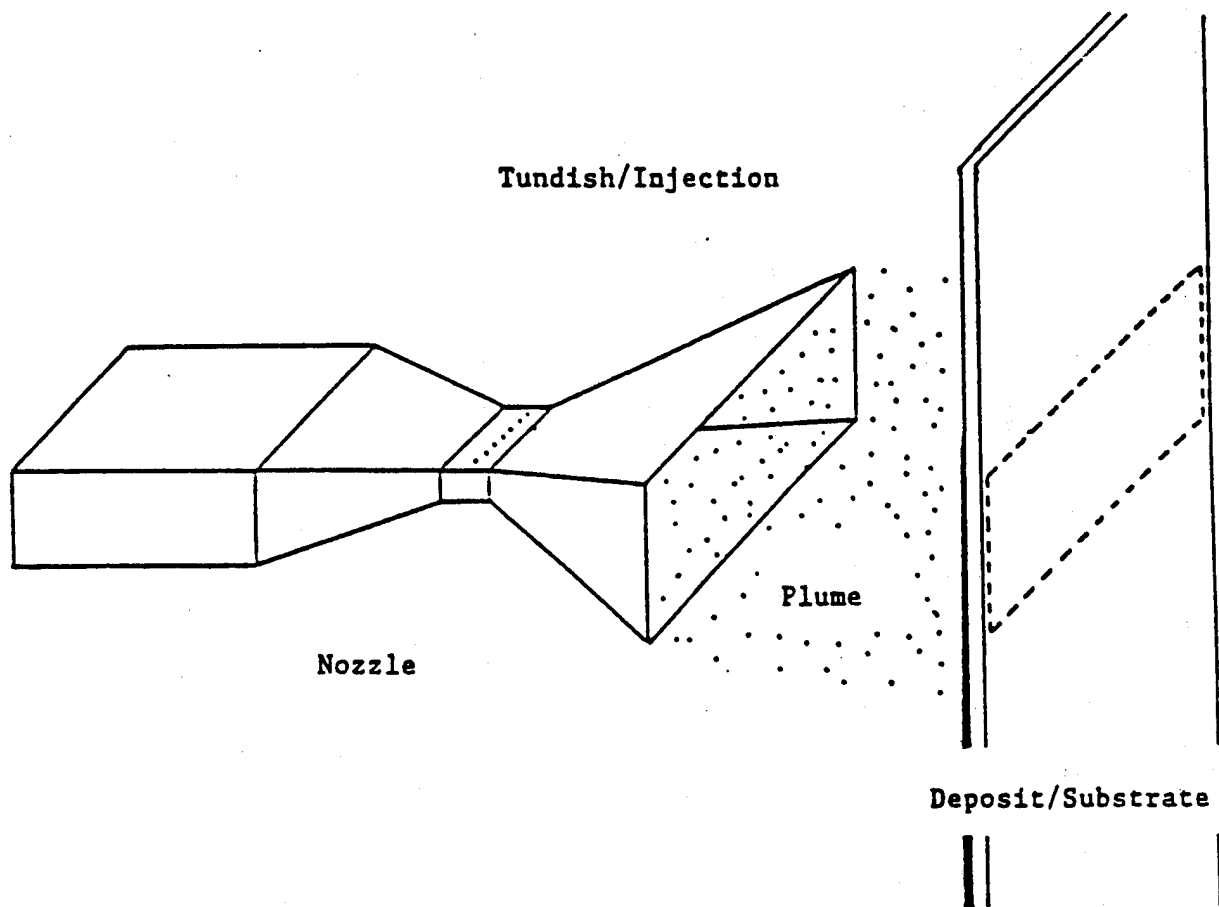
Figure 19. Schematic of Experiment for Quasi One-Dimensional Model.

- Nozzle inlet pressure (absolute) = 145.0 kPa
- Nozzle outlet pressure (absolute) = 86.0 kPa
- Inlet gas temperature = 923.0 K
- Nozzle wall temperature = 1923.0 K
- Gas viscosity = 2.0 N s/m$^2$
- Gas thermal conductivity = 0.0176 W/m·K
- Gas Prandtl number = 0.69
- Nozzle wall relative roughness = 0.01
- Liquid metal injection temperature = 1973.0 K
- Droplet diameter = 25.0 $\mu$m
- Liquid metal specific heat = 700.0 J/kg·K
- Solid metal specific heat = 423.0 J/kg·K
- Metal density = 8387.0 kg/m$^3$
- Metal melting temperature = 1630.0 K
- Metal fusion temperature = 1533.0 K
- Metal heat of fusion = 315.0 J/g
- Depth of liquid metal in tundish = 0.1 m
- Diameter of each injection hole = 0.508 mm
- Number of injection holes = 6
- Discharge coefficient for injection = 0.75
- Pressure (absolute) above liquid metal in tundish = 86.0 kPa
- Tangent of plume divergence half-angle = 0.0524

- Gas specific heat = 518.4 J/kg·K
- Distance from nozzle exit to target = 0.406 m
- Coefficient A in Equation (19) = 0.72 mm/s K$^n$
- Exponent n in Equation (19) = 1.8

As Figure 20 indicates, the gas velocity reaches a maximum in the nozzle, downstream of the throat. The liquid metal droplets are injected with essentially zero velocity (axial) at the end of the nozzle throat (upstream of the maximum gas velocity). The gas velocity decreases sharply across the shock wave and then more gradually. The particles are accelerated or decelerated by the drag force associated with the difference between the velocities of the particle and the gas.

The temperature of the injected liquid metal is higher than the gas temperature, and the metal gradually gives up heat to the gas until the onset of freezing (Figure 21). In this example, freezing starts when the metal is cooled to 1533 K, which occurs at about 0.36 m from the nozzle inlet. Between 0.31 and 0.36 m, the metal is an undercooled liquid, being at temperatures below its equilibrium freezing temperature of 1630 K. The liquid metal in this undercooled state can be thought of as storing an excess of energy associated with its nonequilibrium liquid state. When the metal reaches its freezing temperature, some of the liquid very quickly solidifies, releasing the stored energy in the form of heat that raises the droplet temperature. Some of this heat is transferred to the gas, so the gas temperature also rises at the onset of metal solidification. This happens at about 0.36 m from the nozzle in this example. The gas temperature increase causes expansion of the gas, which results in a slight increase in the gas velocity. Figures 20 through 22 show abrupt increases in the gas velocity, gas temperature, and metal solid fraction at this location. After recalescence, the metal continues to solidify at a much lower (nearly equilibrium) rate, and in doing so continues to give up heat to the gas. The gas temperature in the plume is determined by two competing effects: heating by the relatively hot metal and cooling by the entrainment of relatively cool gas from the environment. The gas pressure (gauge), shown in Figure 23, experiences a large drop in the converging portion and pre-shock diverging portion of the nozzle, followed by a
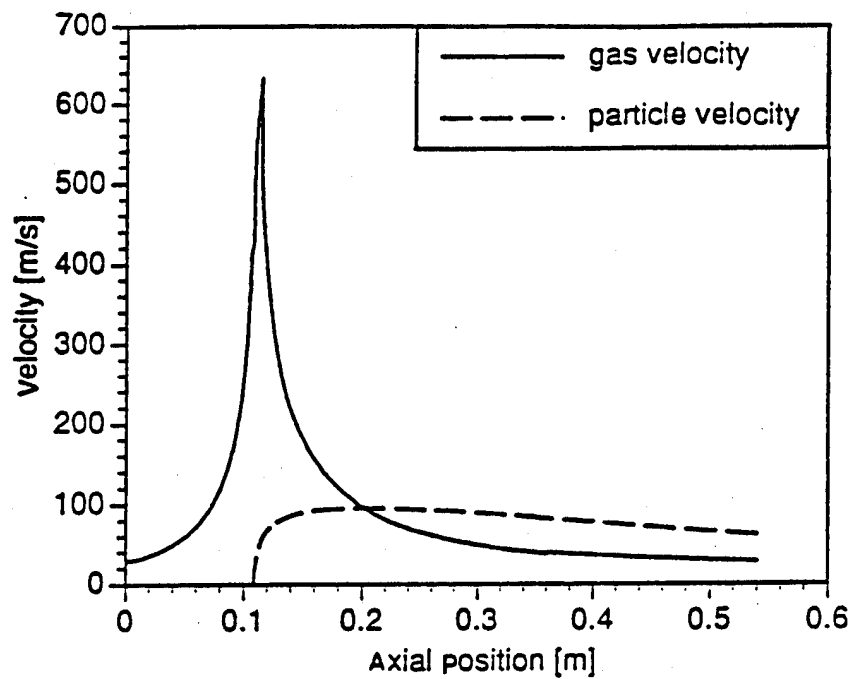
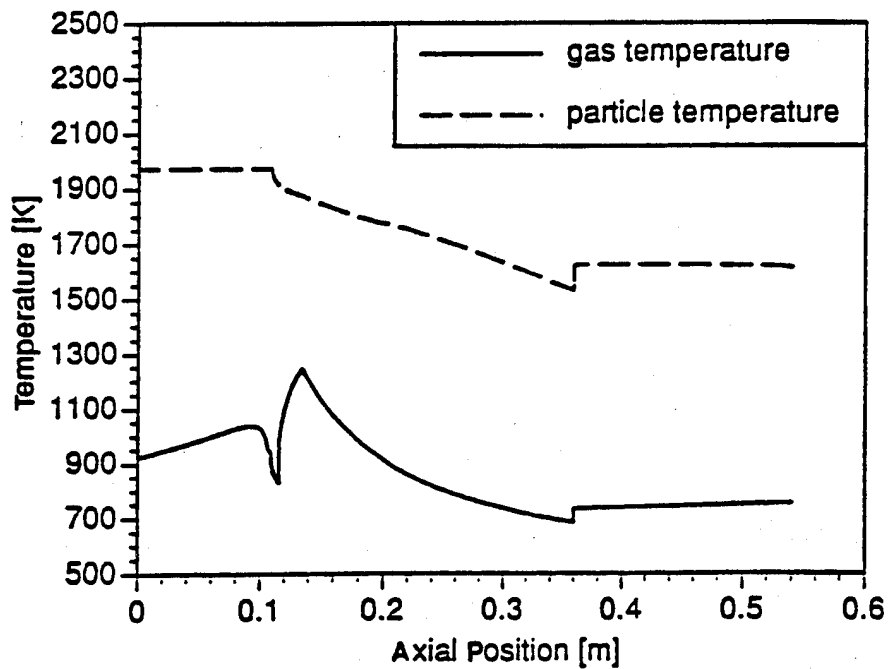Figure 20.  Gas and Particle Velocity Spatial Distribution.



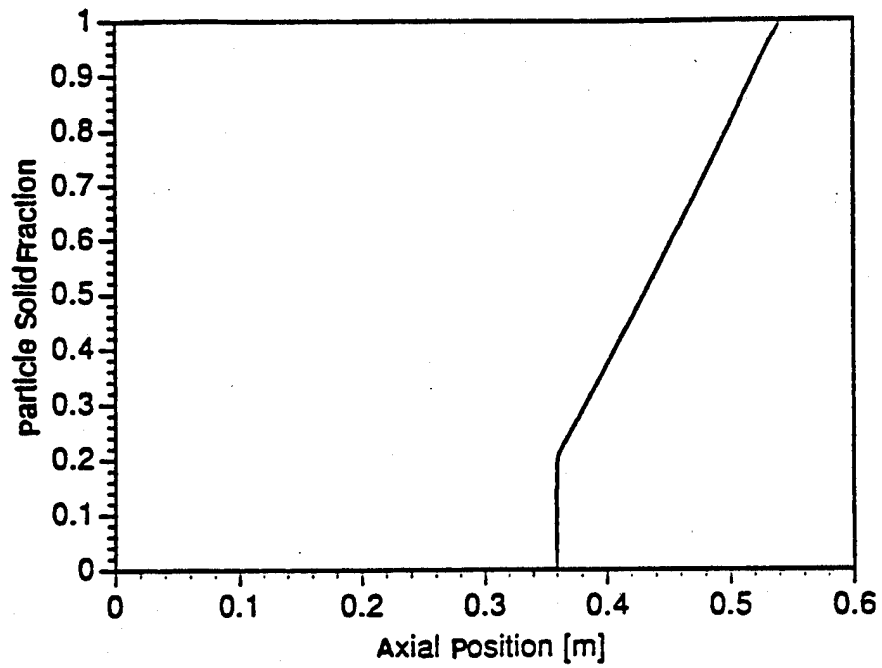Figure 21.  Gas and Particle Temperature Spatial Distribution.

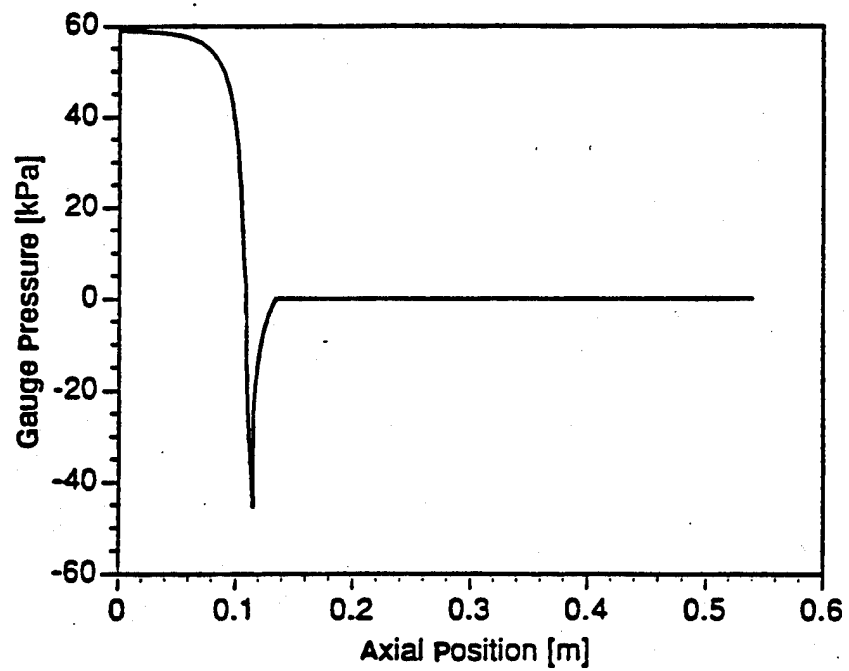Figure 22.   Particle Solid Fraction Spatial Distribution.



Figure 23.   Gas Pressure (gauge) Spatial Distribution.

recovery through the post-shock diverging portion of the nozzle to ambient atmospheric pressure at the nozzle exit. This ambient pressure is, of course, maintained throughout the plume.

In this example, the metal particle is almost completely solid when it impacts the target at 0.54 m. Several things can be done to increase the liquid fraction at impact. One of the most effective is to increase the temperature of the gas in the environment around the plume. For an environment gas temperature of 300 K, as in the example, the droplet solid fraction is 0.995 and its temperature is 1615 K at impact. Raising the environment gas temperature to about 800 K decreases the droplet solid fraction to 0.212 and raises its temperature slightly (not above the melting temperature). Raising the environment gas temperature a little more prevents the metal from solidifying before impact, but the metal is undercooled so that its temperature may be as low as the fusion temperature of 1533 K at impact. Increasing the environment gas temperature above 800 K increases the temperature of the droplet at impact. Clearly, the temperature of the environment gas can have a major effect on the state of the metal at the target.

The size of the injected metal droplets also has a large effect on the state of the metal at impact, as shown in Figure 24. Thus, a spray system must be designed to give an optimum metal droplet size, with allowance for uncontrollable variations in the sizes of the droplets. Figure 24 shows that changes of 5 $\mu$m in the nominal 25 $\mu$m droplet diameter can result in major changes in the solid fraction of the melt on impact.

The initial temperature of the injected liquid metal and the nozzle inlet gas temperature also affect the droplet solid fraction at the target, but these effects are not as dramatic as those of droplet size and environment gas temperature.

The effects of changes in certain parameters that are not as easily controlled are also of interest. Figures 25 and 26 show the effects of variations in two uncontrollable parameters that are expected to be
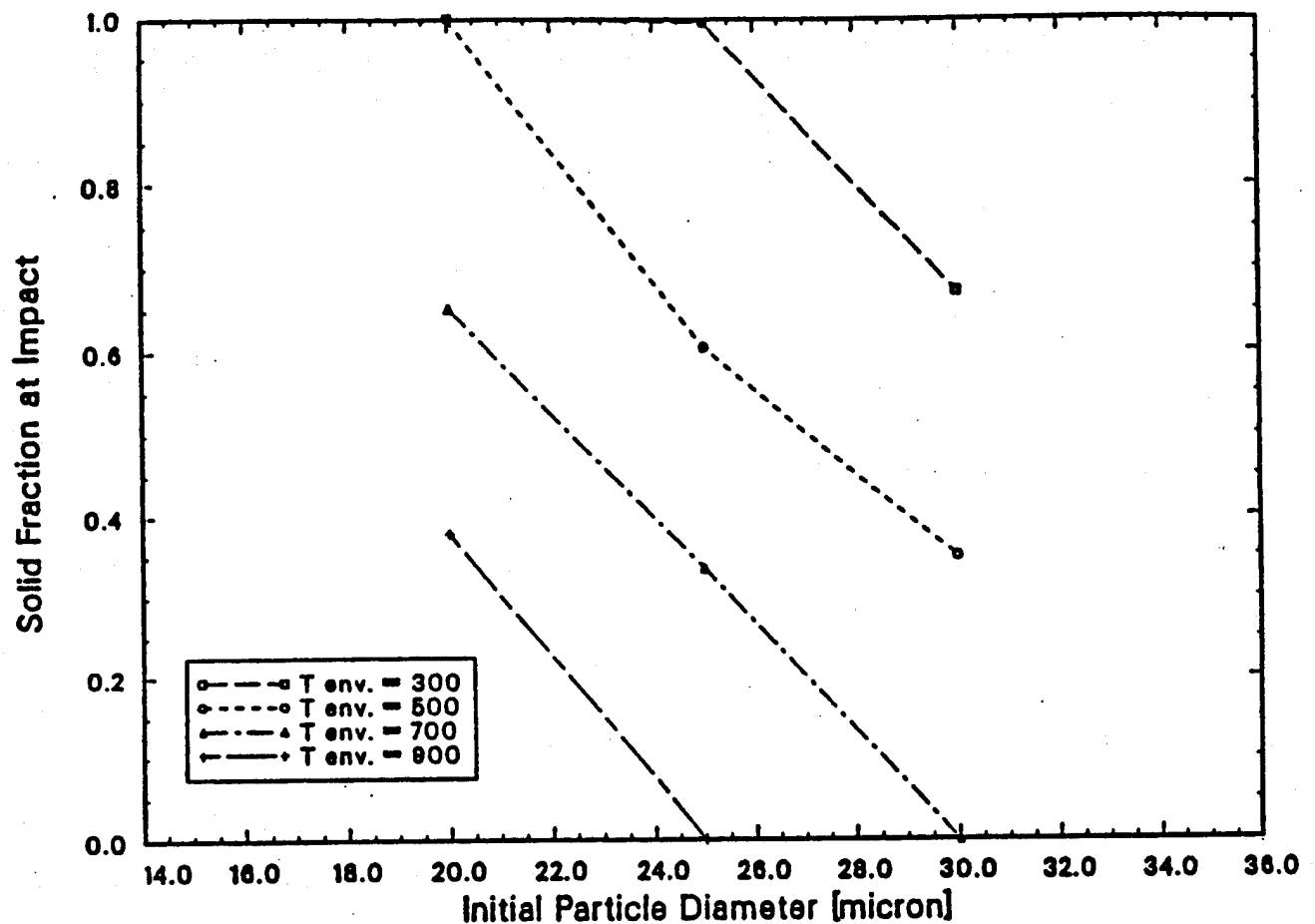
Figure 24. Effect of Droplet Size on Droplet Solid Fraction at Impact for Several Entrained Gas Temperatures.

significant: the liquid metal specific heat and the plume divergence angle (entrainment). These plots indicate the sensitivity to parameter variations, which is useful in determining the margin of error to allow for uncertainties in the uncontrollable parameter values.

While these quasi one-dimensional model studies are useful for identifying trends and obtaining some quantitative data, there are limitations in models this simple. The most obvious limitation is that the model assumes that all variables (temperature, velocity, droplet concentration, entrained gas concentration, etc.) are constant over the local cross-sectional area at each axial location in the nozzle and plume. In reality, these variables may have strongly multidimensional distributions, especially in the injection and diverging regions of the
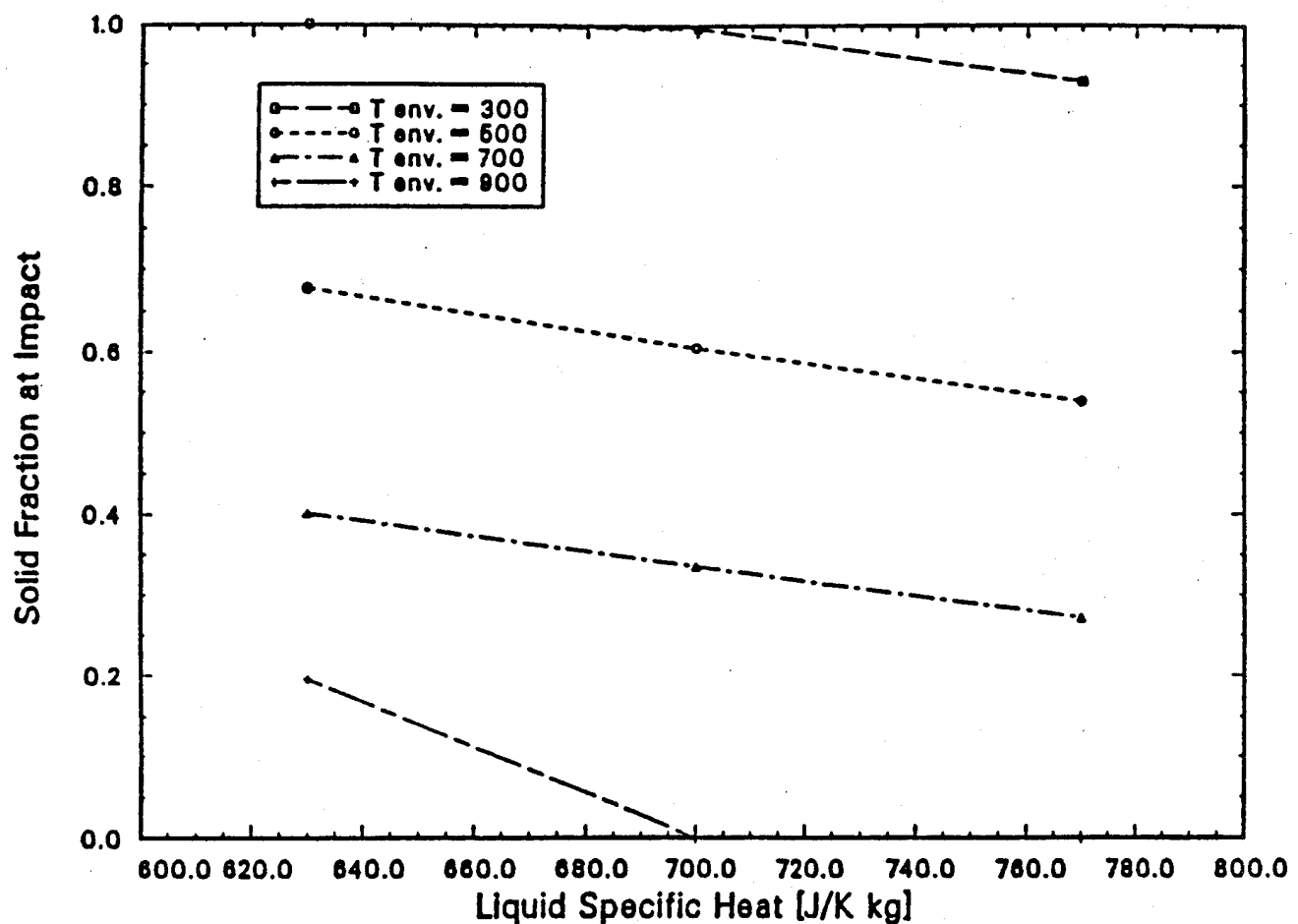
73

Figure 25.    Effect of Droplet Liquid Specific Heat on Droplet Solid
              Fraction at Impact.


nozzle, and plume mixing with environment gas is not ideal. These
limitations must be kept in mind when interpreting the results described
for this model; however, even with these limitations, the one-dimensional
model is very useful in guiding development work.


2.  Two-Dimensional Nozzle Modeling Methodology


        During the course of the related DOE project, several two- and
three-dimensional simulation methodologies were examined for potential use
with high speed compressible, two-phase flows. Because of the relatively
low particulate concentration in the gas stream, the best approach was
concluded to be that of representing the gaseous phase in an Eulerian
fashion with the droplet phase being represented in a Lagrangian manner, as
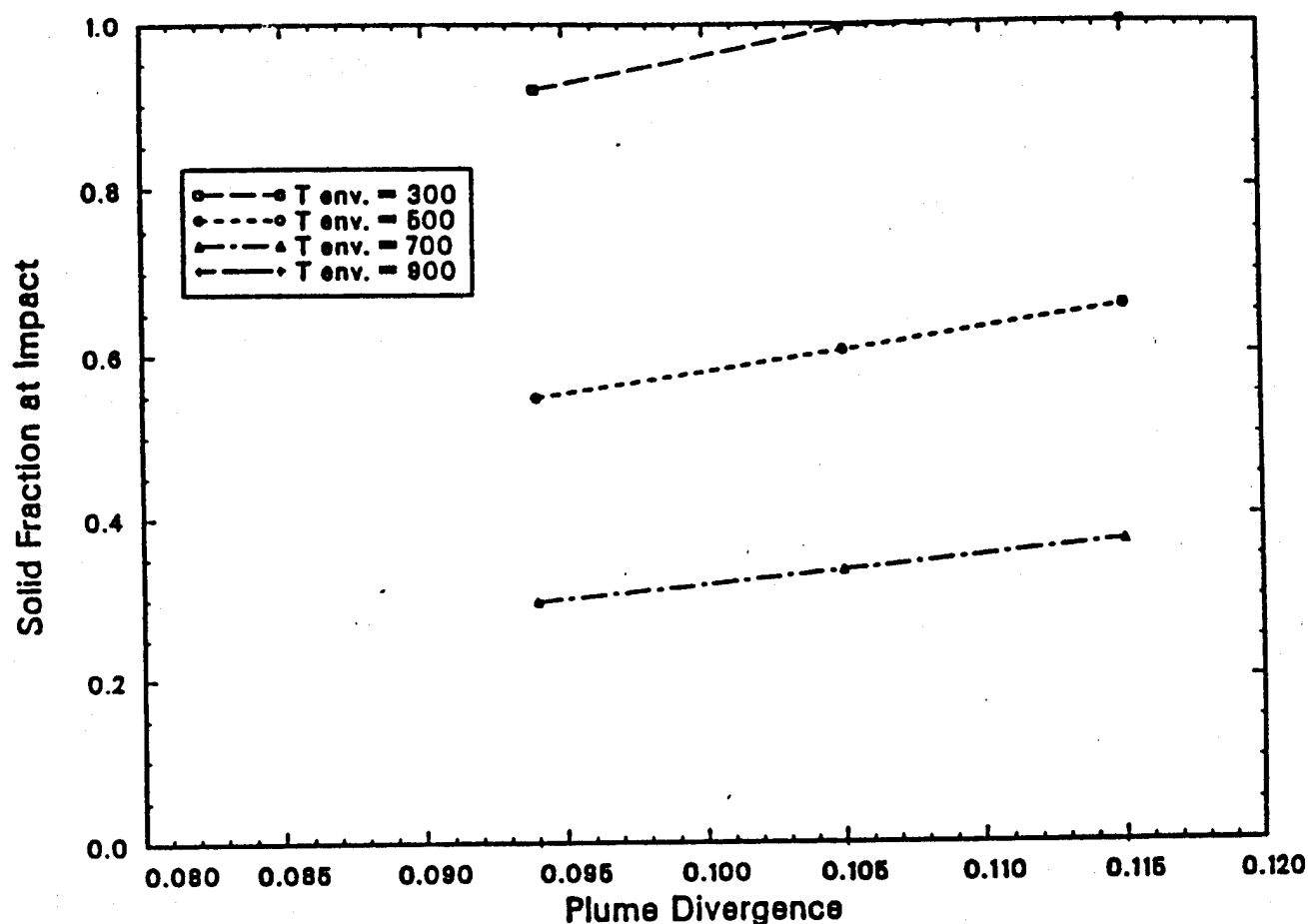
Figure 26. Effect of Plume Divergence Angle (i.e., environment gas entrainment rate) on Droplet Solid Fraction at Impact.

was true of the quasi one-dimensional models. A two-dimensional simulation of the nozzle gas dynamics was carried out using a linearized block implicit numerical technique with a k-e turbulence model. The basic capability to handle a droplet field is in place (some modifications still need to be made); however, at the present time efforts have been primarily focused on the necessary first step of analyzing and understanding the basic gas flow field, disregarding the droplet phase. Representative pressure, density, temperature, dynamic pressure, Mach number, velocity, and particle trace fields for a two-dimensional simulation have been mapped. These results are preliminary.

## 3. Conclusions

The quasi one-dimensional models discussed here are excellent scoping tools and can also be used to rapidly build the investigator's "feel" for the system's response to changes in important variables. They will most certainly prove valuable for the construction of algorithms for the control of spray coating processes. These quasi one-dimensional models give direction to the two- and three-dimensional simulations and serve as a test vehicle for particle/droplet dynamics and energetics submodels.

# SECTION VI
## CONCLUSIONS

A high temperature spray coating system was designed, and cobalt-chromium hardfacing alloys were sprayed successfully at furnace and nozzle temperatures up to 1900°C. The temperature necessary for spraying elemental chromium, 2100°C, was also achieved, but the accelerated degradation of the boron nitride nozzle at these conditions effectively prevented spraying pure chromium. Boron nitride was chosen for the nozzle body material during nozzle development because it is easily machined; however, materials with better service lives are available for fabricating production nozzles. The nozzle's 6-degree entrance and exit contours overcame the high surface tension of the cobalt-chromium alloys so that they were aspirated through the small liquid orifices.

The resistance-based gas heater design proved troublesome. Inductive gas heating with refractory metal elements appears far more suitable for production spray coating systems. The induction furnace performed almost perfectly. Standard zirconia crucibles withstood numerous experiments throughout the Phase II temperature range without significant deterioration from either melt dissolution or reactions with the graphite susceptor. Pure chromium was successfully melted and poured from this furnace at 2100°C.

An economical spray chamber with simple O-ring seals and inert gas purging successfully prevented oxidation of molten metal and sprayed droplets, and isolated laboratory personnel from electrical and particulate hazards. Therefore, no need is envisioned for expensive, time-consuming evacuation-and-backfill approaches in spray coating systems at USAF Air Logistics Centers. A simple purged chamber will also allow standard motor designs to be used for articulating aircraft components in front of the spray plume. Trace amounts of loose particulates ("overspray") were completely filtered from the chamber exhaust, so no hazardous materials were discharged to the environment.

The thin steel strips used as base metal coupons were prepared merely by grit blasting with coarse alundum, with no acid pickling or cathodic cleaning as is typically performed before chrome plating. Spray coating technology thus has the potential to eliminate these cleaning steps and associated liquid wastes, along with the post-plating anneal that removes hydrogen absorbed during these cleaning operations.

The adhesion strength of the cobalt-chromium coatings ranged from approximately 500 to 4200 psi. The lower values were caused by partial delamination from differential thermal stresses and rupturing within the coating layer at locally high concentrations of porosity. Differential thermal stresses can be minimized by uniform preheating of the base metal, which will also foster better wetting of the interface and stronger mechanical bonding. Care must be exercised to retain the required mechanical properties of the base metal. Rupturing will be reduced with future nozzle refinements that provide finer droplets and less gas entrapment, which will also lower interfacial porosity. Achieving consistently high adhesion strength will require optimizing base metal preparation techniques, including cleaning, roughening, and preheating.

Porosity averaged about two area percent, with virtually all values less than five area percent. This surpasses conventional thermal-spraying techniques, and the absence of interconnected porosity assures corrosion resistance is not impaired. Bulk porosity from incomplete splat consolidation was more common on thinner, rapidly cooled coatings, while entrapped gas pores occurred more frequently in nearly molten coatings. Porosity can probably be reduced to the one area percent levels found in Phase I with nozzle modifications that improve droplet breakup and plume uniformity.

Microhardness measurements on Stellite 6 and Coast 64 coatings correlated directly with as-sprayed microstructures. Lower hardness values were obtained from fine dendritic deposits, while much higher values were found in microcrystalline and amorphous material with especially fine dispersions of carbide precipitates. Coatings of Haynes Ultimet (developed

78

for galling resistance) were much softer, due to its much lower carbon content. All sprayed deposits were noticeably harder than weld-overlayed or cast parent stock, with hardness increases as large as 300 percent in the most rapidly solidified deposits. The hardness of the cobalt-chromium coatings ranged from 1100 to 1300 DPH (Vickers), nearly twice as high as the value for electroplated chromium in engineering thicknesses; thus, spray formed coatings are likely to exhibit greatly superior wear resistance. The hardness of spray formed coatings can probably be increased further with finer droplets that solidify even faster and with adjustments to the composition of sprayed alloys, such as increasing the carbon content to increase the amount of hard carbides. However, hardness may be lowered somewhat by composition adjustments to reduce brittleness. Brittle coatings may be prone to fatigue cracking on USAF components.

The one-dimensional heat-transfer model gave valuable insight into the thermal/solidification response of thick coatings that are rapidly deposited. This equilibrium-state, one-dimensional model is not appropriate for thin coatings with slower deposition times, where significant solidification can occur in the droplet splat. The quasi one-dimensional nebulizer models were excellent scoping tools that rapidly provided physical intuition for the system's response to changes in important variables. Such models will prove valuable for constructing algorithms to control the spray coating process and will also supply direction to the two- and three-dimensional simulations and serve as test vehicles for submodels on particle/droplet dynamics and energetics.

## SECTION VII
## RECOMMENDATIONS

The results of Phase II provide ample justification for further
development of the spray coating process as a replacement for chromium
electroplating for eventual implementation at Air Logistics Centers.
Information related to chamber purging, gas heating, nebulizer performance,
nozzle lifetime, base metal preparations, choice of coating alloys, and
computer model development that was learned over the course of Phase II
should provide valuable direction and help to prioritize forthcoming
research studies.

Argon was chosen as the nebulizing and purging gas for Phase II because
liquid argon was conveniently available. The cost of argon is not
significant at the laboratory scale, but cost-effectiveness will be a far
greater concern at ALCs; consequently, nitrogen should be evaluated for
suitability for both purging and nebulizing. Production-scale use of argon
might require gas recycling, while recycling of more economical nitrogen
could probably be avoided. Because of nitrogen's larger heat capacity, it
is also possible that convective cooling rates can be increased further to
maximize benefits of rapid solidification in coating deposits.

As noted several times, the gas heater designs with resistive elements
were prone to premature failures wherever the elements contacted the oxide
insulators. Major difficulties were also encountered in balancing power
and gas flow among the elements. Consequently, this approach should be
abandoned in favor of induction heating. Inductively heating a single,
massive refractory metal heat exchanger could readily achieve gas
temperatures as high as desired without significant risk of failure.

Nozzles of boron nitride were prone to liquid metal erosion at the
tundish base and, at the highest temperatures, to reactions with the
adjacent graphite susceptors that limited their service life. Materials
other than boron nitride will be evaluated after the nozzle geometry is

firmly established. Many different ceramics can be cast into the appropriate shape and machined with diamond tooling, and several refractory metals could be used as susceptors. Alternatively, the nozzle body itself could be fabricated from refractory metal, with quickly replaceable ceramic inserts for the tundish and liquid orifices.

Obtaining consistently high adhesion strength will require more attention to base metal preparation, especially techniques used for roughening and preheating. Grit blasting was shown to provide adequate surface roughness, but the roughening was typically performed several weeks in advance of coating, and no special provisions were made to preserve clean surfaces. Roughening shortly before coating and interim storage in an inert, dust-free environment would likely reduce interfacial porosity and improve mechanical bonding. It is also possible that grit blasting of USAF components might initiate fatigue cracks in the base metal. Such components are commonly shot-peened before chrome plating to build compressive stresses into the base metal surface in order to prevent fatigue problems; it is not known whether or not this technique would provide adequate mechanical bonding with spray coating.

Partial coating delamination from differential thermal stress was occasionally observed on Phase II samples, especially on thicker coatings where the magnitude of edge tapering was greater. A discrete preheating apparatus should be employed to ensure wetting uniformity at the leading plume edge, as well as to minimize shrinkage differences between the coating and base metal.

Carbide reinforcement in the coating appears highly desirable to maximize the advantages of rapid solidification, so Stellite 6 and Coast 64 appear particularly promising as spray coating materials. However, the compositions of these alloys were formulated for weld-overlaying at much lower solidification rates than occur during spray forming. Composition optimization experiments should, therefore, be performed to balance the overall coating properties in spray coated material, especially where it may be necessary to diminish brittle fracture tendencies. Alloys based

upon the nickel-chromium and iron-chromium systems should be evaluated; use of these could reduce thermal contraction mismatches and associated delamination problems. Furthermore, consideration must be given to the hardness of components (such as bearings) that will come into contact with spray coated objects, since wear is always a coupled problem.

Significantly more modeling work should be done for thin coatings with relatively slow deposition rates to incorporate the more complex features that govern splat solidification. Class boundaries delimiting the coatings described by the simple Phase II model and the more complex models are not well defined and will not be until the models are constructed and their results compared with the simple models and related experiments. Work has begun at the INEL on nonequilibrium solidification models based upon a theoretical two-phase mixture approach. It appears that coupling this approach with a rezoning Lagrangian dynamics approach to represent the droplet splat dynamics is a feasible way to pursue this problem. Another approach with strong merit is the quasi-particle method in which droplet splat dynamics are handled not with conventional Cauchy stress models, but rather as a collection of quasi-particles with a Leonard-Jones type stress representation in a pseudo-molecular dynamic fashion. Hybrid methods between these two approaches may also prove feasible. While these methods have never been applied to this type of problem, it is believed that this problem is tractable and necessary to ultimately produce "coatings by design."

Quasi one-dimensional models are inadequate for purposes of optimizing and scaling up the spray nozzle design. Multi-dimensional simulations of the nozzle and plume sprays are critical for the success of Phase III. This ability exists at the INEL in conjunction with the DOE-Office of Industrial Processes, Steel Initiative Program, and it would be most efficient to continue this work in conjunction with or as an extension/expansion of that program.

Pilot- and commercial-scale implementation of a new process, such as spray forming with wear-resistant materials requires a technology base

that, at a minimum, includes quantifiable relationships between process parameters, nozzle and other component design parameters, and product characteristics. Particle diagnostics, available at the INEL Research Center, should be used to quantify the effects of the specific nebulizing gas chosen, gas temperature, gas flow rate (pressure), nozzle design, and liquid metal pressure (head) on droplet size, velocity, and temperature. These measurements should be used to verify and refine modeling predictions. Particle measurements near the impact zone should be related to heat transport into and out of the base metal to quantify cooling rate and thermal cycling, which could affect the mechanical properties of the base metal as well as the deposit. Particle measurements should also be related to deposit characteristics such as grain size, porosity, hardness, adhesion to the base metal, and dimensional uniformity. Such measurements could also be used to verify deposition models. A nozzle with a single, circular liquid orifice should be investigated for applications such as repairing wear grooves in bearing races where uniform coating thickness may not be desirable. Significantly different nozzles have been developed recently in other programs at this laboratory that produce much smaller droplet size and more uniform coatings. These concepts should be evaluated for this application using the scientific method described above.

# SECTION VIII
## REFERENCES

1. Watson, L.D. et al., "Nozzle-Aspirated Metal Forming," paper presented at the Metallurgical Society's International Symposium on Casting of Near Net Shape Products, Honolulu, HI, 13-17 November, 1988.

2. Alvarez, J.L. and Watson, L.D., "Apparatus and Method for Spraying Liquid Materials," U.S. Patent No. 4,919,853, 24 April 1990.

3. Ploger, S.A. et al., Spray Coating of Metals, Phase I: Feasibility of Concept, USAF Report ESL-TR-89-61, May 1990.

4. Dibble, M.A., "Coatings Cover New Ground," Machine Design, pp. 40-48, 22 June 1989.

5. "Surface Cleaning, Finishing and Coating," The Metals Handbook, 9th ed., vol. 5, American Society for Metals, 1984.

6. Berry, R.A. and Crowe, C.T., "Quasi One-Dimensional Nozzle and Plume Models for Spray Forming," to be published.

7. Clift, R. et al., Bubbles, Drops, and Particles, Academic Press, New York, 1978.

8. Hunter, S.C. et al., Gas-Particle Nozzle Flows with Reaction and Particle Size Change, AIAA-81-0037, 1981.

9. Bird, R.B. et al., Transport Phenomena, John Wiley, New York, 1960.